NMR Characterization of the Dynamics of Biomacromolecules

Arthur G. Palmer, III*

Department of Biochemistry and Molecular Biophysics, Columbia University, 630 West 168th Street, New York, New York 10032

Received November 10, 2003

Contents

1. Introduction

Function in biological systems is exquisitely dependent on spatial and temporal changes in biomacromolecules. Innumerable biological processes ultimately rely on transduction of information through conformational changes in proteins and nucleic acids associated with folding and assembly, ligand binding and molecular recognition, and catalysis. A central problem in understanding biological processes at a molecular level is the elucidation of how the active conformation of biomacromolecules is achieved on time scales necessary for function. Recent technological developments have revolutionized the range of spectroscopic and other approaches available for the study of dynamic processes in biomacromolecules; however, NMR spectroscopy has a unique capacity to investigate dynamic properties of molecules over a range of different time scales with atomic resolution in both solution and solid states.[1]

* Phone: (212) 305-8675. Fax: (212) 305-6949. E-mail: agp6@columbia.edu.

Arthur G. Palmer, III is Professor of Biochemistry and Molecular Biophysics at Columbia University. He received his Ph.D. in Chemistry with Nancy L. Thompson from the University of North Carolina at Chapel Hill. He was a National Science Foundation Postdoctoral Fellow with Peter E. Wright at the Scripps Research Institute. The focus of his research is NMR spin relaxation and molecular motions in biological macromolecules.

Solution NMR spectroscopy studies of biomolecular dynamics have become widespread because of the range of motional time scales that are accessible, the spatial resolution offered by isotopic labeling of proteins and nucleic acids coupled with 2D and 3D spectroscopy, and the relentless advancement in experimental and computational methods, illustrated in Figure 1. The purpose of this review is to describe the principal applications of spin relaxation methods for investigating conformational dynamic processes in proteins and nucleic acids. Experimental techniques used for measuring spin relaxation rate constants have been reviewed recently;[2−4] therefore, the present review focuses on the interpretation of spin relaxation data, rather than its acquisition. By the same token, fundamental derivations of relaxation theory are not presented; comprehensive reviews are available.[5−7] Spin relaxation is not the only NMR phenomenon available for the investigation of conformational dynamics in biological macromolecules; other established and emerging techniques are based on amide proton exchange,[8,9] scalar coupling constants,[10] and residual dipole coupling constants.[11−17] Other reviews in this special issue describe applications of these other methods.

Nuclear spin relaxation results from time-dependent stochastic modulation of spin Hamiltonians,

10.1021/cr030413t CCC: $48.50
Published on Web 06/26/2004

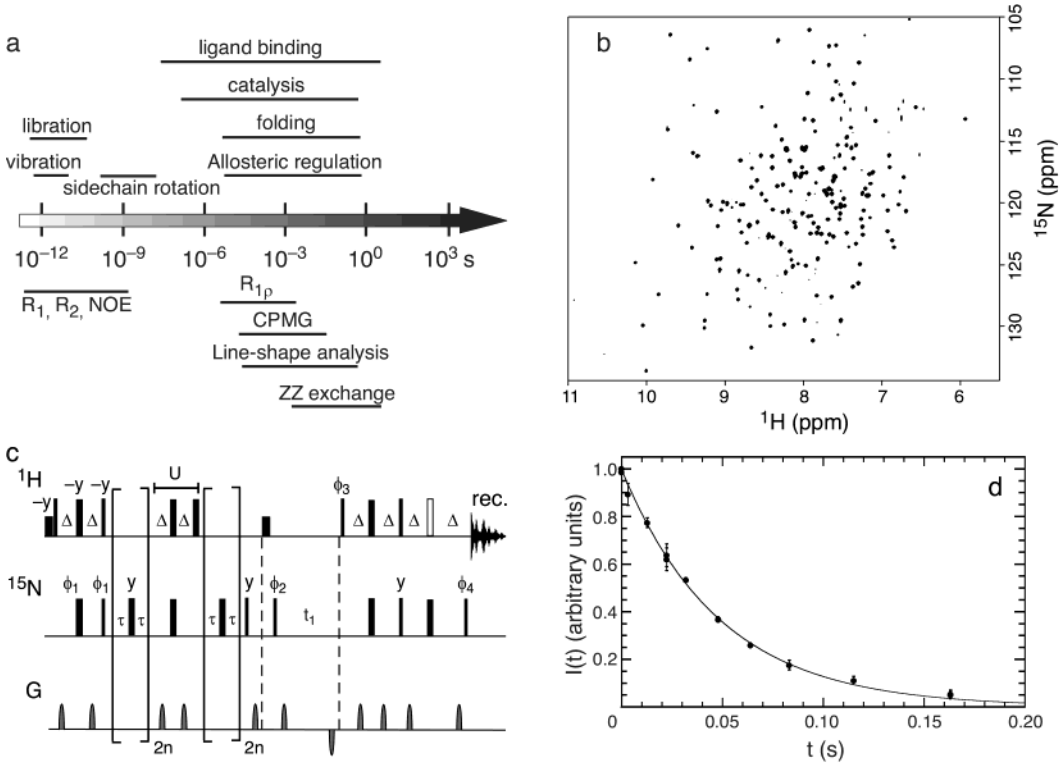

Figure 1. NMR methods for macromolecular dynamics. (a) Time scales for protein dynamics and NMR techniques. Protein motions and NMR spin relaxation techniques for studying them span more than 12 orders of magnitude in time scale. (b) Resolution of 2D NMR spectroscopy. $^{1}H-^{15}N$ TROSY correlation spectrum for 2.0 mM [U-83% ^{2}H, U-98% ^{15}N] yeast triosephosphate isomerase (TIM) acquired at 800 MHz (pH 5.8, T = 293 K). TIM is a symmetric dimer with a total molecular mass of 54 kD and 248 amino acid residues per monomer. Correlations for nearly all backbone amide moeities can be resolved in the spectrum. (c) New methods for characterizing protein dynamics. As an illustrative example, the TROSY−CPMG pulse sequence for measuring conformational and chemical exchange in ^{15}N-labeled proteins is shown.[211] All pulses are x-phase unless otherwise indicated. Narrow and wide bars depict 90° and 180° pulses, respectively; short wide bars indicate selective 90° pulses; and the open bar represents a 3−9−19 or other water-selective 180° pulse. Delays are Δ = 2.7 ms, $\tau = 0.5\ \tau_{cp}$. The phase cycle for the first FID is $\phi_1 = 4(x), 4(-x)$; $\phi_2 = -y, y, x, -x$; $\phi_3 = y$; $\phi_4 = x$; receiver = x, −x, −y, y, −x, x, y, −y. The phase cycle for the second FID is $\phi_1 = 4(x), 4(-x)$; $\phi_2 = -y, y, x, -x$; $\phi_3 = -y$; $\phi_4 = -x$; receiver = −x, x, −y, y, x, −x, y, −y. Gradients (G) are used for suppression of artifacts and water radiation damping. (d) Site-specific relaxation rate constants.[15]N TROSY−CPMG relaxation data for Thr 172 in TIM is shown. The data were acquired using the pulse sequence of (c) using $\tau_{cp} = 0.8$ ms. The relaxation rate constant obtained from the fitted curve (solid line) is 20.39 ± 0.36 s^{-1}.

including the dipole−dipole, chemical shift anisotropy (CSA), quadrupolar, isotropic chemical shift, and scalar coupling Hamiltonians.[18] Relaxation rate constants have maximum magnitudes on the order of $\langle\delta\omega^2\rangle\tau_c$, in which $\langle\delta\omega^2\rangle$ is the mean square variation in the local magnetic field resulting from deviation of the stochastic Hamiltonian from its average value and τ_c is the correlation time for the stochastic process. Assuming, optimistically, that relaxation rate constants between 10^{-1} and 10^{3} s^{-1} can be measured experimentally, the time scale of a dynamic process that can be characterized by spin relaxation methods depends directly on the magnitude of the variation in the spin Hamiltonian modulated by the dynamic process. Thus, motions on ps−ns time scales are accessible to spin relaxation resulting from modulation of dipole−dipole, CSA, and quadrupolar Hamiltonians; motions on μs−ms time scales are accessible to spin relaxation resulting from modulation of isotropic chemical shifts. The magnitude of the variation in isotropic scalar coupling constants in proteins and nucleic acids, on the order of 10 Hz, is too small to have proven broadly useful as a direct relaxation probe of molecular dynamics. However, observation of averaged values of scalar coupling constants provides evidence of dynamic processes that are too fast to serve as efficient relaxation mechanisms.[10]

2. Relaxation Techniques for Fast Time Scale Dynamics

Conformational dynamics on time scales comparable to or faster than the overall rotational correlation times for biomacromolecules influence spin relaxation rate constants by stochastically modulating dipole−dipole, CSA, and quadrupolar Hamiltonians. The majority of applications of spin relaxation methods in proteins utilize the amide ^{15}N spin as a probe of backbone motions[19] and the ^{2}H spin in CH2D methyl group isotopomers as a probe of side chain dynamics.[20,21] Relaxation of the carbonyl ^{13}C spin provides a second probe of the dynamics of the backbone peptide plane.[22]

2.1. Laboratory Frame Relaxation Rate Constants

The relaxation rate constants for the S (=^{15}N or ^{13}C, typically) spin in an IS spin system subject to

dipole−dipole interactions with the I (=^{1}H or ^{13}C, typically) spin and to CSA of the S spin are given by[18,23]

$$R_1 = (d^2/4)[J(\omega_I - \omega_S) + 3J(\omega_S) + 6J(\omega_I + \omega_S)] + c^2 J(\omega_S) \quad (1)$$

$$R_2 = (d^2/8)[4J(0) + J(\omega_I - \omega_S) + 3J(\omega_S) + 6J(\omega_I) + 6J(\omega_I + \omega_S)] + (c^2/6)[4J(0) + 3J(\omega_S)] \quad (2)$$

$$\sigma_{IS} = (d^2/4)[6J(\omega_I + \omega_S) - J(\omega_I - \omega_S)] \quad (3)$$

in which R_1 is the spin−lattice or longitudinal relaxation rate constant; R_2 is the spin−spin or transverse relaxation rate constant; σ_{IS} is the dipole−dipole cross-relaxation rate constant; $d = (\mu_0 h\gamma_I\gamma_S/8\pi^2)\langle r_{IS}^{-3}\rangle$; $c = \Delta\sigma\omega_S/\sqrt{3}$; μ_0 is the permeability of free space; h is Planck's constant; γ_I and γ_S are the gyromagnetic ratios of the I and S spins, respectively; r_{IS} is the I−S bond length; ω_I and ω_S are the Larmor frequencies of the I and S spins, respectively; $\Delta\sigma$ is the CSA of the S spin; and the chemical shift tensor is assumed to be axially symmetric. For the quadrupolar interaction of a spin-1 nucleus, such as ^{2}H[18,20,23]

$$R_1 = 3\xi^2[J(\omega_D) + 4J(2\omega_D)] \quad (4)$$

$$R_2 = (3\xi^2/2)[3J(0) + 5J(\omega_D) + 2J(2\omega_D)] \quad (5)$$

$$R_{1Q} = 9\xi^2 J(\omega_D) \quad (6)$$

$$R_{2z} = (3\xi^2/2)[3J(0) + J(\omega_D) + 2J(2\omega_D)] \quad (7)$$

$$R_{DQ} = 3\xi^2[J(\omega_D) + 2J(2\omega_D)] \quad (8)$$

in which R_{1Q} is the relaxation rate constant for quadrupolar order, represented by the operator $3I_z^2 - 2$; R_{2z} is the relaxation rate constant for antiphase coherence, represented by the operator $I^+I_z + I_zI^+$; R_{DQ} is the relaxation rate constant for double-quantum coherence, $\xi = \pi e^2qQ/(2h)$ is the quadrupole coupling constant; e is the charge on the electron; eq is the principal value of the electric field gradient tensor; Q is the nuclear quadrupole moment and ω_D is the ^{2}H Larmor frequency.

The spectral density function describes the frequency spectrum of the stochastic process and is given by[18]

$$J(\omega) = \frac{1}{5}\int_0^\infty \langle P_2[\mu(0)\cdot\mu(t)]\rangle \cos(\omega t)\, dt \quad (9)$$

in which $P_2[x] = (3x^2 - 1)/2$, $\mu(t)$ is a unit vector defining the orientation of the unique axis of the relaxation interaction in the laboratory reference frame, and $\langle\ \rangle$ represents an ensemble average. The vector $\mu(t)$ is parallel to the internuclear vector for dipolar-coupled nuclei and to the symmetry axis of axially symmetric CSA or quadrupolar tensors. The expressions given in eqs 1 and 2 use the same spectral density function for both the dipole−dipole and CSA relaxation mechanisms. This is tantamount to assuming that the CSA tensor is axially symmetric with the symmetry axis oriented parallel to the dipole−dipole internuclear vector. For ^{15}N, the angle between the CSA and dipole−dipole tensors is ∼17°.[24] The effect of noncollinearity between the CSA and dipole tensors has been discussed.[24,25] An asymmetric CSA tensor can be represented by two orthogonal axially symmetric tensors.

Analyzing dipolar, chemical shift anisotropy, and quadrupolar relaxation rate constants requires accurate knowledge of the values of r_{IS}, $\Delta\sigma$, and ζ, respectively. Experimental and theoretical calculations suggest that the combinations of $\Delta\sigma = -163$ ppm and $r_{NH} = 1.04$ Å should be used for the ^{15}N spin.[26,27] Site-specific variations in $\Delta\sigma$ values for ^{15}N spins have been investigated theoretically and experimentally.[28−32] The variations in ^{15}N and ^{13}CO CSA values observed in solution are similar to the ranges (∼5−10 ppm) observed in small peptides by solid-state NMR. Quadrupolar coupling constants for methyl groups appear to be very uniform with an average value of $e^2qQ/h = 167$ MHz.[33]

2.2. Spectral Density Mapping

Relaxation rate constants are linear combinations of $J(\omega)$ sampled at the eigenfrequencies of the spin system. Consequently, discrete values of $J(\omega)$ can be obtained formally by inverting the systems of equations given in eqs 1−3 and 4−7. In practice, the relaxation rate constants can be analyzed directly by using programs such as ModelFree[34] or indirectly by first determining $J(\omega)$. In the latter case, the procedure to obtain $J(\omega)$ from the experimental relaxation data is called spectral density mapping.[35,36]

For the backbone amide ^{15}N spin, a particularly elegant and robust approach, termed reduced spectral density mapping, is applicable.[37−40] The linear combinations of $J(\omega_H - \omega_S)$, $J(\omega_H)$, and $J(\omega_H + \omega_S)$ that appear in eqs 1−3 are approximated to first order by a single term of the form $\alpha J(\beta\omega_H)$, in which α and β are constants. The resulting dipolar and CSA relaxation rate constants are given by

$$R_1 = (d^2/4)\,[3J(\omega_N) + 7J(\beta_1\omega_H)] + c^2 J(\omega_N) \quad (10)$$

$$R_2 = (d^2/8)\,[4J(0) + 3J(\omega_N) + 13J(\beta_2\omega_H)] + (c^2/6)\,[4J(0) + 3J(\omega_N)] \quad (11)$$

$$\sigma_{NH} = (d^2/4)\,5J(\beta_3\omega_H) \quad (12)$$

in which $\beta_1 = 0.921$, $\beta_2 = 0.955$, and $\beta_3 = 0.87$. The system of equations can be solved for $J(0)$, $J(\omega_N)$, and $J(\beta_3\omega_H)$ in one of three ways: assuming $J(\beta_i\omega_H) = J(\beta_3\omega_H)$, approximating $J(\beta_i\omega_H) = (\beta_3/\beta_i)^2 J(\beta_3\omega_H)$, or extrapolating values of $J(\beta_i\omega_H)$ from the empirical static magnetic field dependence of $J(\beta_3\omega_H)$.

As discussed in section 3, the transverse relaxation rate constant may contain additional contributions from chemical exchange processes that arise from μs−ms exchange of spins between magnetic environments, R_{ex}. As a result, values of $J(0)$ obtained from eq 11 will be overestimated. If data is available at

multiple static magnetic fields, B_0, then $J(0)$ can be determined from[40,41]

$$\Gamma = R_2 - \frac{1}{2}R_1 - (3d^2/4)J(\omega_H) = (d^2/2)J(0) + (2\gamma_N{}^2\Delta\sigma^2 J(0)/9 + \Theta_{ex})B_0{}^2 \quad (13)$$

in which the result $R_{ex} = \Theta_{ex}\boldsymbol{B}_0{}^2$ has been used. The intercept of a least-squares fit of Γ versus the static magnetic field strength, $B_0{}^2$, yields $J(0)$ directly. Approaches for identifying ^{15}N spins affected by chemical exchange processes have been reviewed.[42]

For the ^{2}H spin, the quadrupolar relaxation mechanism is much more efficient than other relaxation mechanisms, including the ^{2}H−^{13}C dipole−dipole interaction and chemical exchange processes. Consequently, contributions to relaxation other than the quadrupolar mechanism can be neglected for the relaxation rate constants given in eqs 4−8. The relaxation rate constants given in these equations depend only on three widely separated values of the spectral density function: $J(0)$, $J(\omega_D)$, and $J(2\omega_D)$. These equations can be inverted without making any additional assumptions. Consequently, spectral density mapping is simplified compared with the ^{15}N spin.

Thus, at each static magnetic field for which spin relaxation data are recorded, the backbone spectral density function for ^{15}N spin is sampled at $J(0)$, $J(\omega_N)$, and $J(0.87\omega_H)$ and the spectral density for the ^{2}H spin is sampled at $J(0)$, $J(\omega_D)$, and $J(2\omega_D)$. This coarse sampling can be improved somewhat by recording data at multiple static magnetic field strengths; for moderate sized (<20 kD) biomacromolecules, data acquisition between 400 MHz (9.4 T) and 900 MHz (21.1 T) is feasible.

2.3. Model-Free Formalism

The relaxation data or spectral density values are most commonly analyzed by fitting simple "model-free" functional forms for $J(\omega)$ containing a limited number of free parameters to the relaxation or spectral density data.[43−46] Other approaches for analyzing ^{13}C and ^{15}N relaxation data have been proposed.[47−54]

For a macromolecule with an axially symmetric rotational diffusion tensor, the model-free spectral density function is given by[44,55,56]

$$J(\omega) = \frac{2}{5}\sum_{j=0}^{2} A_j \left[\frac{S^2\tau_j}{1 + \omega^2\tau_j{}^2} + \frac{(1 - S^2)\tau_j'}{1 + \omega^2\tau_j'^2} \right] \quad (14)$$

in which $\tau_j{}^{-1} = 6D_\perp - j^2(D_\perp - D_\parallel)$, $D_\parallel$ and $D_\perp$ are the components of a axially symmetric diffusion tensor; $A_0 = (3\cos^2\theta - 1)^2/4$, $A_1 = 3\sin^2\theta\cos^2\theta$, $A_2 = (3/4)\sin^4\theta$, the angle between the unique axis of the diffusion tensor and the equilibrium orientation of the $\mu(t)$ vector is θ, S^2 is the square of the generalized order parameter characterizing the equilibrium distribution of orientations of $\mu(t)$ in a molecular reference frame, $\tau_j' = (1/\tau_j + 1/\tau_e)^{-1}$, and τ_e is the internal correlation time for motions of $\mu(t)$ in a molecular reference frame. If rotational diffusion is isotropic, then $D_\parallel = D_\perp = D$, $\Sigma A_j = 1$, and $\tau_m = \tau_j = 1/(6D)$ is the isotropic overall rotational correlation time of the protein. In this case, eq 14 reduces to the original formulation of Lipari and Szabo[44]

$$J(\omega) = \frac{S^2\tau_m}{1 + \omega^2\tau_m{}^2} + \frac{(1 - S^2)\tau}{1 + \omega^2\tau^2} \quad (15)$$

with $\tau = (1/\tau_m + 1/\tau_e)^{-1}$. More complex expressions are necessary for a fully asymmetric diffusion tensor ($D_{xx} \neq D_{yy} \neq D_{zz}$). The model-free formalism is essentially identical to the "two-step" model proposed by Halle and Wennerström.[55] The relationship between the parameters of eq 14 is illustrated schematically in Figure 2.

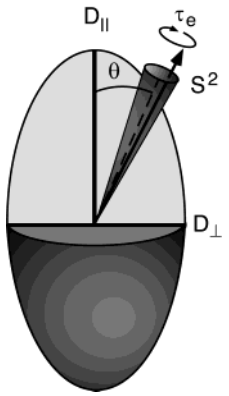

Figure 2. Model-free parameters for axially symmetric diffusion tensor. The diffusion constants are $D_\parallel$ for diffusion around the symmetry axis of the diffusion tensor and $D_\perp$ for diffusion around the two orthogonal axes. The equilibrium position of the I−S bond vector is oriented at an angle θ with respect to the symmetry axis of the diffusion tensor. Local dynamics of the bond vector are depicted as stochastic motions within the shaded cone and are characterized by the order parameter, S^2, and the effective internal correlation time, τ_e.

If two internal motional processes are necessary to describe relaxation for sites exhibiting complex dynamic properties, then[43]

$$J(\omega) = \frac{2}{5}S_f{}^2\sum_{j=0}^{2} A_j \left[\frac{S_s{}^2\tau_j}{1 + \omega^2\tau_j{}^2} + \frac{(1 - S_s{}^2)\tau_j'}{1 + \omega^2\tau_j'^2} \right] \quad (16)$$

in which $S^2 = S_f{}^2 S_s{}^2$, S_f is the order parameter for motions on a fast time scale (τ_f < 10 ps), S_s is the order parameter for motions on a slow time scale ($\tau_f < \tau_s < \tau_m$), and $\tau_j' = (1/\tau_j + 1/\tau_s)^{-1}$. The expression of eq 16 is formally equivalent to the very anisotropic local motion (VALM) limit of the slowly relaxing local structure (SRLS) model;[52] in this case, $S_s = S_{SRLS}$ and S_f formally is identified with $(3\cos^2\beta - 1)/2$, in which β is the angle between the molecular diffusion axis and the bond vector. The dependence of the relaxation rate constants on the model-free parameters for the original Lipari-Szabo approach are illustrated in Figure 3.

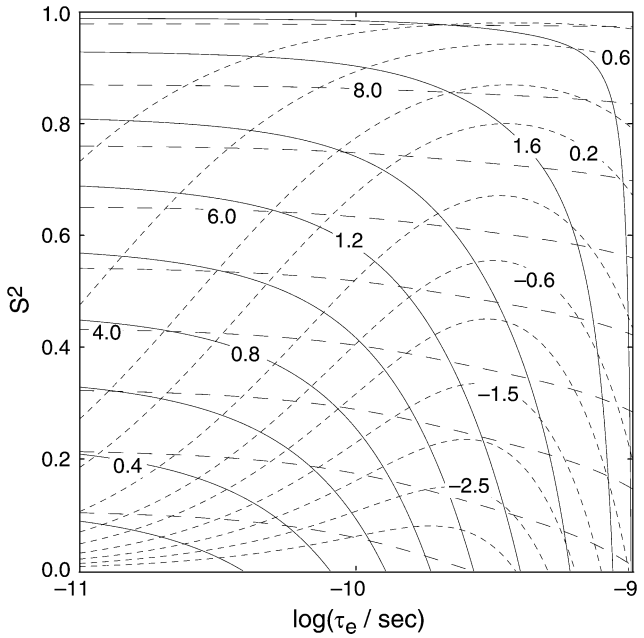

Figure 3. Dependence of ^{15}N relaxation rate constants on model-free parameters S^2 and τ_e. Calculations were performed using eq 15 and $\tau_m = 8.0$ ns. (—) R_1 contour lines are drawn at 0.2, 0.4, 0.6, 0.8, 1.0, 1.2, 1.4, 1.6, and 1.7 s^{-1}. (- — -) R_2 contour lines are drawn at 1.0, 2.0, 3.0, 4.0, 5.0, 6.0, 7.0, 8.0 and 9.0 s^{-1}. (- — -) $\{^1H\}-^{15}N$ NOE contour lines are drawn at −3.0, −2.5, −2.0, −1.5, −1.0, −0.6, −0.2, 0.2, 0.4, 0.6, and 0.7. A subset of the contours are labeled for clarity.

For a moderately anisotropic molecule with $0.5 < D_{\|}/D_{\perp} < 2$,[57] eqs 14 and 16 can be approximated by

$$J(\omega) \approx \frac{2}{5}\left[\frac{S^2\tau_1}{1+\omega^2{\tau_1}^2} + \frac{(1-S^2)\tau_1'}{1+\omega^2{\tau_1'}^2}\right] \quad (17)$$

$$J(\omega) \approx \frac{2}{5}{S_f}^2\left[\frac{{S_s}^2\tau_1}{1+\omega^2{\tau_1}^2} + \frac{(1-{S_s}^2)\tau_1'}{1+\omega^2{\tau_1'}^2}\right] \quad (18)$$

in which τ_1 is the overall rotational correlation time sensed locally by the ith spin

$$(6\tau_1)^{-1} = e_i^{\mathrm{T}}\mathbf{Q}e_i \quad (19)$$

e_i are the direction cosines for the orientation of the interaction vector $\mu(t)$ in the principal axis frame of the diffusion tensor; $\mathbf{Q}$ is diagonal with elements $Q_{xx} = (D_{yy} + D_{zz})/2$, $Q_{yy} = (D_{xx} + D_{zz})/2$, and $Q_{zz} = (D_{xx} + D_{yy})/2$; and $\tau_1' = (1/\tau_1 + 1/\tau_e)^{-1}$ or $\tau_1' = (1/\tau_1 + 1/\tau_s)^{-1}$. For an axially symmetric diffusion tensor in the principal axis system

$$D_i = D_{iso} - P_2(\cos\theta)[D_{\|} - D_{\perp}]/3 \quad (20)$$

in which $D_{iso} = (D_{\|} + 2D_{\perp})/3$ provides one simple relationship between the local overall rotational correlation time and the diffusion tensor.[58−60] If diffusion is isotropic, then $\tau_1 = \tau_m$, and eq 17 is identical to the original expression of Lipari and Szabo. The approach of eqs 17 and 19 formally separates the determination of the diffusion tensor from the determination of the other model-free parameters because the sets $\{\tau_1, S^2, \tau_e\}$ or $\{\tau_1, {S_f}^2, {S_s}^2, \tau_s\}$ are determined independently for each spin. This is particularly useful if spectral density data are obtained at more than one static magnetic field strength.

Relaxation in methyl groups results from rotational averaging due to fast rotation of the methyl group around the methyl symmetry axis, motions of the methyl symmetry axis, and overall rotational tumbling. In long side chain amino acids in particular, motions of the methyl symmetry axis may result from both fast (librational) and slow (rotameric transitions) processes. Skrynnikov and co-workers have utilized the spectral density function[21]

$$J(\omega) \approx \frac{2}{5}P_2[\cos\theta_{CH}]\left[\frac{S^2\tau_{eff}}{1+\omega^2{\tau_{eff}}^2} + \frac{(1-S^2)\tau}{1+\omega^2\tau^2}\right] \quad (21)$$

in which $\tau = (1/\tau_{eff} + 1/\tau_e)^{-1}$, τ_{eff} represents the combined effect of the slow local motion of the methyl symmetry axis and (isotropic) overall rotational diffusion, $P_2[\cos\theta_{CH}]$ reflects fast averaging due to methyl rotation, and $\theta_{CH} = 70.5°$ is the angle between the C−H vector and the methyl symmetry axis. In this model, S^2, τ_e characterize the fast dynamics of the methyl symmetry axis. In the absence of slow motions, $\tau_{eff} = \tau_m$ and eq 21 is formally equivalent to the Lipari-Szabo formalism, eq 15, modified for fast methyl rotation.

Practical aspects of data analysis, including model selection and error analysis, are not discussed herein.[34,61−65] In general, rotational diffusion tensors and generalized order parameters are reliably determined by NMR relaxation measurements. However τ_e or τ_s can be characterized precisely only over a relatively narrow range unless high quality data are available at multiple static magnetic field strengths. In most cases, $\tau_e < 30$ ps and τ_e, $\tau_s \rightarrow \tau_m$ are poorly determined. Examples of the results of reduced spectral density mapping and fitting to the model free formalism are given in Figure 4.

2.4. Generalized Order Parameter

The generalized order parameter is a measure of the equilibrium distribution of orientations of the vector $\mu(t)$ in a molecular reference frame[44]

$$S^2 = (4\pi/5)\sum_{m=-2}^{2}|\langle Y_2^m(\theta,\phi)\rangle|^2 \quad (22)$$

in which $Y_2^m(\theta,\phi)$ are spherical harmonic functions of the orientations of $\mu(t)$ in a molecular reference frame, defined by $\{\theta, \phi\}$. The ensemble average is defined by

$$\langle Y_2^m(\theta,\phi)\rangle = \int_0^{2\pi}\int_0^{\pi} p(\theta,\phi)Y_2^m(\theta,\phi)\sin\theta\,d\theta\,d\phi \quad (23)$$

in which the probability, $p(\theta, \phi)$, of finding the N−H vector in a given orientation $\{\theta, \phi\}$ is given by

$$p(\theta,\phi) = \exp[-\beta W(\theta,\phi)]/\int_0^{2\pi}\int_0^{\pi}\exp[-\beta W(\theta,\phi)]\sin\theta\,d\theta\,d\phi \quad (24)$$

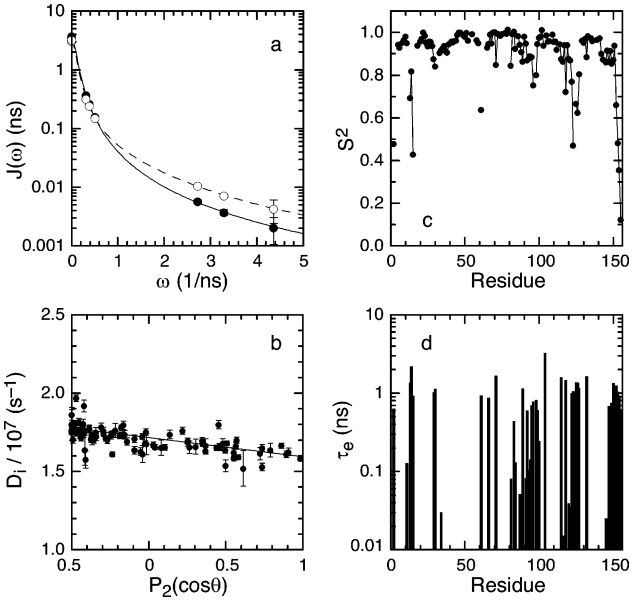

Figure 4. Spectral density data and model-free analysis for backbone amide ^{15}N spins in *E. coli* ribonuclease H. (a) $J(\omega)$ for (●, —) Gly 20 and (○, - - -) Val 98 obtained from reduced spectral density mapping using ^{15}N R_1, R_2, NOE, transverse ^{1}H−^{15}N dipole/^{15}N CSA relaxation interference, and longitudinal ^{1}H−^{15}N dipole/^{15}N CSA relaxation interference data recorded at three static magnetic fields (11.7, 14.1 and 18.8 T).[30] Model free results give $S^2 = 0.96 \pm 0.01$ for Gly 20 and $S_f^2 = 0.90 \pm 0.01$, $S_s^2 = 0.87 \pm 0.01$, and $\tau_e = 0.8 \pm 0.1$ ns for Val 98. (b) Values of the local overall rotational diffusion constants, D_i are graphed versus P_2(cos θ), in which θ is the polar angle describing the orientation of the N−H bond vector in the principal axis system of the diffusion tensor. The diffusion tensor has principal values $D_{iso} = 1.72 \times 10^7$ s^{-1} and $D_\parallel/D_\perp = 1.23$. Model-free results for (c) S^2 and (d) τ_e are illustrated as a function of amino acid residue number. The secondary structure elements of ribonuclease H are five α-helices (residues 43−58, 71−80, 81−88, 100−112, and 127−142), and a five β-strands (residues 4−13, 18−27, 32−42, 64−69, and 115−120). All relaxation data were recorded at a temperature of 300 K. Analysis was performed using a N−H bond length of 1.04 Å and a ^{15}N CSA of −163 ppm.

$\beta = 1/(k_B T)$, k_B is the Boltzmann constant, and $W(\theta,\phi)$ is the potential of mean force (PMF) that constrains the orientation of $\mu(t)$. The definition of S^2 does not depend on a particular motional model and ranges from unity for vectors with fixed orientations to zero for vectors with isotropic orientational distributions. If motion of $\mu(t)$ is modeled as restricted diffusion in a cone, then S^2 is given by[44]

$$S^2 = [\cos\theta_0 (1 + \cos\theta_0)/2]^2 \qquad (25)$$

and the amplitude of motion is characterized by the cone semiangle, θ_0. In an alternative conceptualization, the Gaussian axial fluctuation (GAF) model,[66,67] the vector diffuses within a parabolic potential on the surface of a cone and S^2 is given by

$$S^2 = 1 - 3\sin^2\theta \{\cos^2\theta (1 - \exp[-\sigma_f^2]) + 0.25 \sin^2\theta (1 - \exp[-4\sigma_f^2])\} \qquad (26)$$

in which θ is the (fixed) angle between $\mu(t)$ and the director axis for the motion and σ_f is the standard deviation of the fluctuation in the azimuthal angle.

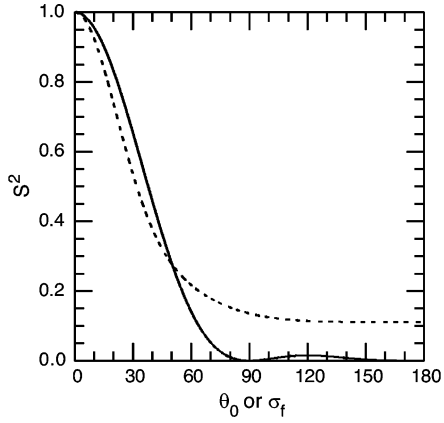

Figure 5. Order parameters for simple motional models. The value of S^2 is graphed as a function of θ_0 (—) calculated using eq 25 and σ_f (- — -) calculated using eq 26 and θ = 70.5°.

Equation 26 reduces to $S^2 = 1 - 3\sin^2\theta\sigma_f^2$ for small fluctuations and to $S^2 = P_2[\cos\theta]^2$ for large fluctuations. The relationships between S^2 and the distribution of conformations is shown in Figure 5. Statistical correlations in a database of N−H S^2 values for 20 proteins have been described,[68] an analytical model has been developed that relates values of the N−H S^2 to close contacts between the H^N and carbonyl oxygen atoms of the corresponding peptide plane,[69] and correlations between backbone ^{15}N order parameters for different sequence positions have been examined through mutagenesis.[70]

Changes in S^2 upon ligand binding or conformational transition in a biological macromolecule reflect altered flexibility and consequent changes in conformational entropy. Order parameters can be used to estimate an upper bound for the change in the Gibbs' free energy, ΔG, or the entropy, ΔS_p, resulting from conformational restriction[71−73]

$$\Delta G = -k_B T \sum_n \ln\left(\frac{1 - S_{n2}^2}{1 - S_{n1}^2}\right) \qquad (27)$$

$$\Delta S_p = -k_B \sum_n \ln\left(\frac{3 - (1 - 8S_{n2})^{1/2}}{3 - (1 - 8S_{n1})^{1/2}}\right) \qquad (28)$$

in which S_{nm} is the order parameter for the nth spin in the mth state and the summation extends over all affected nuclei. These equations neglect correlations between the dynamical properties of the spins included in the summations and include only the entropic effects of the part of the conformational ensemble characterized by the set of order parameters. The first limitation has been investigated through molecular dynamics simulations.[74] The second limitation arises because the spectral density function is insensitive to motions that do not reorient the vector $\mu(t)$. The backbone ^{13}CO CSA tensor and the ^{13}CO−^{13}C$^\alpha$ dipole−dipole tensor in proteins have a different orientation in the peptide plane than does the ^{15}N−^{1}H dipole−dipole tensor. Combined relaxation studies of ^{15}N and ^{13}CO spins suggests that additional motions of the peptide plane may affect

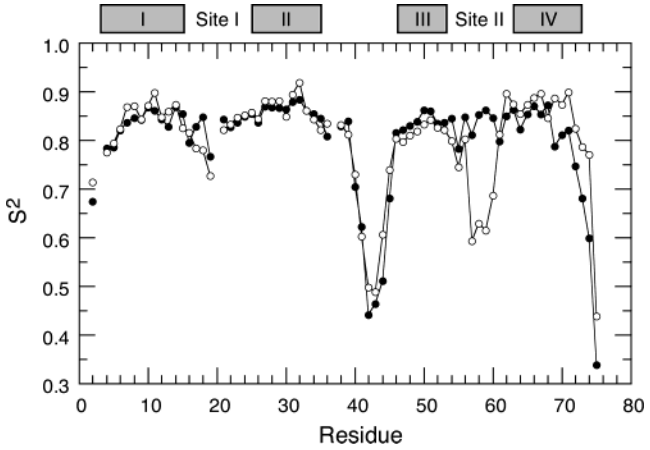

Figure 6. Comparison of the generalized order parameters for (○) apo and (●) calcium loaded calbindin D_{9k}.[76] The order parameters are shown as a function of sequence. The error bars are on the order of the size of the plotted points. The location of the four helices in the protein are indicated by gray rectangles. The calcium binding sites are labeled as site I and site II. Using eq 27, an estimate of $\Delta G = \sim 13$ kJ mol^{-1} is obtained for the difference in free energy between the apo and $(Ca^{2+})_2$ states.

^{13}CO, but not ^{15}N, relaxation properties.[22,75] The first application of these approaches used eq 27 to quantify entropic changes in the protein calbindin D_{9k} resulting from binding of Ca^{2+};[71,76] the order parameters for the apo and $(Ca^{2+})_2$ states of calbindin D_{9k} are shown in Figure 6.

The temperature dependence of S provides information on the temperature dependence of the PMF.[77−79] The parameter, Λ, has been introduced to characterize the temperature dependence of the order parameter S[80]

$$\Lambda = \frac{d \ln(1 - S)}{d \ln T} \tag{29}$$

The definition of Λ has the property that $\Lambda < 1$ for a temperature-independent harmonic PMF. Experimental results give $\Lambda > 1$,[80] and molecular dynamics simulations suggest that, for ordered backbone sites in proteins, the PMF depends on temperature.[81] If the PMF, $W(\theta, \phi, T)$, is assumed to depend linearly on temperature

$$W(\theta,\phi,T) = W_0[1 + \alpha(T - T_0)]f(\theta,\phi) \tag{30}$$

in which W_0 is the strength of the potential, $\alpha = (\partial \ln W(\theta,\phi,T)/\partial T)_{T=T_0}$ and $f(\theta,\phi)$ expresses the dependence of the PMF on $\{\theta, \phi\}$. In this case

$$\frac{\Lambda}{\Lambda_0} = 1 - \alpha T_0 \tag{31}$$

in which Λ_0 is the value of Λ calculated for $\alpha = 0$, that is, for a PMF that does not depend on temperature. Computational simulations suggest that the PMF is described for N−H bond vectors in residues in stable secondary structural elements, by $f(\theta,\phi) = \theta^2$; thus, Λ_0 can be calculated using a quadratic potential energy function.[81] Examples of the experimental temperature dependence of the order parameters for the small protein HP36 are shown in Figure 7. Other applications have used the temperature dependence of S to obtain information about contributions to heat capacity from conformational fluctuations.[79,82−84]

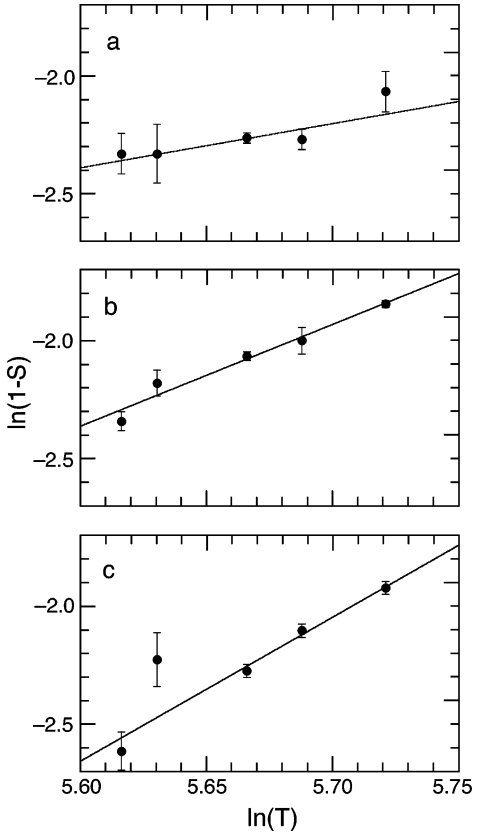

Figure 7. Representative plots of $\ln(1 - S)$ versus $\ln(T/1$ K) for residues (a) 49, (b) 53, and (c) 68 in HP36.[80] Temperature is in units of K. Solid lines are best linear fits of the data, yielding slopes Λ equal to (a) 1.87 ± 0.97, (b) 4.31 ± 0.31, and (c) 6.10 ± 0.57. An average value of $\alpha W_0 = -0.4$ kJ mol^{-1} K^{-1} is obtained for HP36 from eq 31.

2.5. Diffusion Tensor and Domain Orientation

Measurements of the rotational diffusion tensors of macromolecules from NMR spin relaxation, using approaches based on eqs 14 and 17 for example, provides experimental information about overall hydrodynamic properties. Although hydrodynamic information also is available from measurements of translational diffusion by NMR,[85] rotational diffusion is more sensitive to details of molecular shape. Advances in programs for modeling hydrodynamic properties of proteins using "bead" models have facilitated the interpretation of experimental data.[86,87] In proteins consisting of multiple folded domains, diffusion tensors measured for the individual domains can suggest the degree to which hydrodynamic motions of the two domains are independent and can serve to constrain structural models for the protein.[57,60,88−91] Spin relaxation approaches for characterizing relative domain motion have been described.[92−94] Measurement of residual dipolar coupling constants provides an alternative approach to determining domain orientation in macromolecules.[89,90,95,96]

3. Relaxation Techniques for Slow Time Scale Dynamics

Chemical exchange is a ubiquitous phenomenon in NMR spectroscopy that provides information on conformational and chemical kinetic process occurring on μs−s time scales. Chemical exchange is the manifestation of processes that modulate isotropic chemical shifts by altering the magnetic environments of spins. The main experimental techniques for quantifying chemical exchange are longitudinal magnetization exchange,[48] line shape analysis,[97] CPMG relaxation dispersion,[98] and $R_1\rho$ relaxation dispersion.[98] These techniques are most commonly applied to ^{1}H, ^{13}C, ^{15}N, and ^{31}P spins in biological macromolecules.[3]

3.1. Bloch-McConnell Equations

Chemical exchange between n sites (chemical or conformational states) is described by the reaction scheme

$$A_1 \underset{k_{21}}{\overset{k_{12}}{\rightleftharpoons}} A_2, \quad A_1 \underset{k_{31}}{\overset{k_{13}}{\rightleftharpoons}} A_3, \quad \ldots A_{n-1} \underset{k_{n(n-1)}}{\overset{k_{(n-1)n}}{\rightleftharpoons}} A_n \tag{32}$$

in which k_{ij} is the first-order rate constant for transitions from state i to j. Ligand-binding or oligomerization reactions are accommodated by defining the appropriate pseudo-first-order rate constants. The evolution of the density operator is governed by the Stochastic Liouville equation

$$\frac{\mathrm{d}\sigma(t)}{\mathrm{d}t} = (\Lambda + \Xi)\sigma(t) + \mathbf{C}_0 \tag{33}$$

in which $\sigma(t)$=$(\sigma_1(t), \sigma_2(t), \ldots \sigma_n(t))^{\mathrm{T}}$, $\sigma_k(t)$ is the density operator for spins in the kth site

$$\Lambda = \begin{bmatrix} \mathbf{L}_1 & 0 & \cdots & 0 \\ 0 & \mathbf{L}_2 & \cdots & 0 \\ \vdots & \vdots & \ddots & \vdots \\ 0 & 0 & \cdots & \mathbf{L}_n \end{bmatrix}$$

$$\Xi = \Gamma \otimes \mathbf{E} \tag{34}$$

$\mathbf{L}_k = -i\mathscr{L}_k + \mathbf{W}_k$, $\mathscr{L}_k$ is the Liouvillian for the spins in the kth site, $\mathbf{W}_k$ is the relaxation superoperator for spins in the kth site, $\mathbf{C}_0 = (-\mathbf{W}_1\sigma_{01}, -\mathbf{W}_2\sigma_{02} \ldots -\mathbf{W}_n\sigma_{0n})^{\mathrm{T}}$, σ_{0k} is the equilibrium density operator for spins in the kth site, $\mathbf{E}$ is the identity matrix, and Γ is the exchange matrix with elements

$$\Gamma_{ij} = k_{ji}$$

$$\Gamma_{jj} = -\sum_{\substack{k=1 \\ k\neq j}}^{n} k_{jk} \tag{35}$$

In the following, the constant term $\mathbf{C}_0$ is ignored; this is equivalent to treating $\sigma(t)$ as the deviation of the density operator from its steady-state value $\sigma_{ss} = -(\Lambda + \Xi)^{-1}\mathbf{C}_0$.

The exchange matrix can be symmetrized by the similarity transformation $\Gamma' = \mathbf{S}\Gamma\mathbf{S}^{-1}$ with $S_{kj} = \delta_{kj}p_k^{-1/2}$, in which p_k is the equilibrium fractional population of the kth site. Consequently, eq 33 can be transformed using the matrix $\mathbf{S}\otimes\mathbf{E}$

$$\frac{\mathrm{d}\sigma'(t)}{\mathrm{d}t} = (\Lambda + \Xi')\sigma'(t) \tag{36}$$

The Laplace transform of $\sigma'(t)$ is given by

$$\tilde{\sigma}'(s) = \int_0^\infty \sigma'(t)\mathrm{e}^{-st}\,\mathrm{d}t \tag{37}$$

which allows eq 36 to be solved in the Laplace domain as[99,100]

$$\tilde{\sigma}'(s) = (s - \Lambda + \Xi')^{-1}\sigma'(0) = \mathbf{K}\sigma'(0) \tag{38}$$

If the initial conditions satisfy $\sigma_k(0) = p_k\sigma(0)$, then the average density operator in the Laplace domain is given by

$$\langle\tilde{\sigma}(s)\rangle = \langle\psi_0|\tilde{\sigma}'(s) = \langle\psi_0|\mathbf{K}|\psi_0\rangle\sigma(0) \tag{39}$$

in which $|\psi_0\rangle = [p_1^{1/2}, p_2^{1/2}, \ldots, p_n^{1/2}]^T\otimes\mathbf{E}$. In the absence of an applied radio frequency field, the frequency domain spectrum is obtained from eq 39 by making the identification $s = i\omega$.

For uncoupled spins described by a macroscopic magnetization, the Bloch-McConnell equations[101] are obtained by replacing $\sigma_k(t)$ by $\langle\mathbf{M}_k\rangle(t)$ = Trace$\{\sigma_k(t)\mathbf{M}_k\}$in eq 33. In the rotating frame of reference, if $\mathbf{M}_k = (M_{xk}, M_{yk}, M_{zk})^T$ are the Cartesian Bloch magnetization components, then

$$\mathbf{L}_k = \begin{bmatrix} -R_{2k}^0 & -\Omega_k & 0 \\ \Omega_k & -R_{2k}^0 & -\omega_1 \\ 0 & \omega_1 & -R_{1k}^0 \end{bmatrix} \tag{40}$$

in which Ω_k, R_{1k}^0, and R_{2k}^0 are the resonance offset, longitudinal relaxation rate constant, and transverse relaxation rate constant for spins in the kth site and ω_1 is the amplitude of an applied radio frequency (rf) field, assumed to have x-phase for convenience. The relaxation rate constants R_{1k}^0 and R_{2k}^0 are given by expressions for R_1 and R_2 for dipole−dipole, CSA, and quadrupolar relaxation given in section II. Thus

$$\langle\tilde{\mathbf{M}}(s)\rangle = \langle\psi_0|\tilde{\mathbf{M}}'(s) = \langle\psi_0|\mathbf{K}|\psi_0\rangle\mathbf{M}(0) \tag{41}$$

3.2. Evolution in the Absence of rf Fields

Within the formalism of the Bloch McConnell equations, free precession evolution of transverse magnetization and evolution of longitudinal magnetization are described by the above equations with $\omega_1 = 0$. In this case, the basis $\mathbf{M}_k = (M_k,^+, M_k^-, M_{zk})^{\mathrm{T}}$ gives

$$\mathbf{L}_k = \begin{bmatrix} i\Omega_k - R_{2k}^0 & 0 & 0 \\ 0 & i\Omega_k - R_{2k}^0 & 0 \\ 0 & 0 & -R_{1k}^0 \end{bmatrix} \tag{42}$$

which is diagonal. Thus, the different magnetization components evolve independently. In the absence of

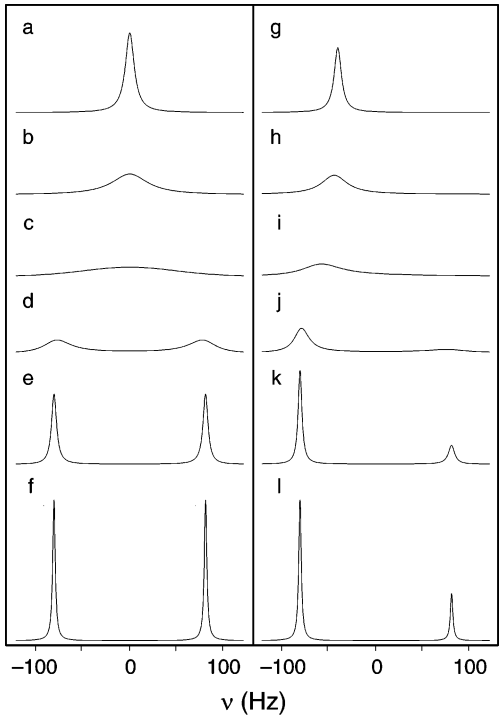

Figure 8. Chemical exchange line shapes. (a−f) Symmetric exchange with $p_1 = p_2 = 0.5$. (g−l) Exchange with skewed populations $p_1 = 0.75$ and $p_2 = 0.25$. Values of k_{ex} are (a, g) 10000, (b, h) 2000, (c, i) 900, (d, j) 200, (e, k) 20, and (f, l) 0.0 s^{-1}. The spectra are simulated with $R_2^0 = 10$ s^{-1} and $\Delta\omega/2\pi = 180$ Hz. Spectra were calculated using eq 43.

an applied rf field, the frequency domain spectrum is given by

$$\langle \boldsymbol{M}^+(\omega)\rangle = \langle \psi_0|\{i(\omega - \Omega) + \rho_2 - \Gamma'\}^{-1}|\psi_0\rangle M^+(0) \quad (43)$$

in which $\Omega_{jk} = \delta_{jk}\Omega_k$ and $\rho_{2jk} = \delta_{jk}R_{2k}^0$. In general, differences between R_{2k}^0 are unimportant when $|\Delta R_{2k}^0| = |R_{2k}^0 - \bar{R}_2^0| \ll |\Gamma_{kk}|$; this is normally a good assumption except for very slow exchange and R_{2k}^0 can be replaced by $\bar{R}_2^0$. This approximation is made in the following when appropriate. Line shape analysis is a classical approach for analyzing exchange processes in NMR spectroscopy.[97,102,103] Computer optimization of the parameters in eq 43 is utilized to fit the experimental NMR spectrum.

Numerous approximate solutions to the Bloch−McConnell equations are known. For fast exchange between n sites, only a single, population-averaged resonance is observed in the free-precession spectrum. The transverse relaxation rate constant for this resonance is given by[104]

$$R_2 = \bar{R}_2{}^0 + \sum_{k=2}^{n} \langle u_1|\omega|u_k\rangle^2/\kappa_k \quad (44)$$

in which $\bar{R}_2^0$ is the population-averaged transverse relaxation rate constant in the absence of exchange and u_k and κ_k are the eigenvectors and absolute values of the eigenvalues of Γ'. For very slow exchange, n resolved resonances are observed with

$$R_{2k} = R_{2k}^0 - \Gamma_{kk} \quad (45)$$

Exchange between two sites

$$A_1 \underset{k_{21}}{\overset{k_{12}}{\rightleftharpoons}} A_2 \quad (46)$$

provides the simplest illustrative example. Simulated frequency domain spectra calculated using eq 43 for two site exchange are shown in Figure 8. The chemical shift time scale is defined by the relationship between k_{ex} and $\Delta\omega$, in which $k_{ex} = k_{12} + k_{21}$ and $\Delta\omega = \Omega_2 - \Omega_1$. When $k_{ex} < \Delta\omega$, exchange is slow on the chemical shift time scale and two resolved resonances are observed in the NMR spectrum. When $k_{ex} > \Delta\omega$, exchange is fast on the chemical shift time scale and single population-averaged resonance is observed. Intermediate exchange is obtained when $k_{ex} \approx \Delta\omega$ and coalescence of the resonance lines is observed.

The exact relaxation rate constant and precession frequency for the dominant resonance signal are given by[105,106]

$$R_{21} = \bar{R}_2{}^0 + \frac{k_{ex}}{2} - \frac{1}{\sqrt{8}}\{k_{ex}{}^2 - \Delta\omega^2 + [(k_{ex}{}^2 + \Delta\omega^2)^2 - 16p_1p_2\Delta\omega^2k_{ex}{}^2]^{1/2}\}^{1/2} \quad (47)$$

$$\Omega_{1ex} = \frac{\Omega_1 + \Omega_2}{2} - \frac{1}{\sqrt{8}}\{\Delta\omega^2 - k_{ex}{}^2 + [(k_{ex}{}^2 + \Delta\omega^2)^2 - 16p_1p_2\Delta\omega^2k_{ex}{}^2]^{1/2}\}^{1/2} \quad (48)$$

in which $R_{21}^0 = R_{22}^0 = \bar{R}_2^0$ and $p_1 > p_2$. For fast exchange, the simple form obtained from eqs 44 or 47 is

$$R_2 = \bar{R}_2{}^0 + p_1p_2\Delta\omega^2/k_{ex} \quad (49)$$

and $\Omega_{1ex} = \bar{\Omega} = p_1\Omega_1 + p_2\Omega_2$. For highly skewed site populations, $p_1 \gg p_2$[107]

$$R_{21} = \bar{R}_2{}^0 + p_2k_{ex}\left[\frac{\Delta\omega^2}{p_1{}^2k_{ex}{}^2 + \Delta\omega^2}\right] \quad (50)$$

$$\Omega_{1ex} = \bar{\Omega} + p_2\Delta\omega\left[\frac{p_1p_2k_{ex}{}^2 - \Delta\omega^2}{p_1{}^2k_{ex}{}^2 + \Delta\omega^2}\right] \quad (51)$$

The approximations of eqs 50 and 51 are compared to the exact results of eqs 47 and 48 in Figure 9. The approximation is accurate for $p_2 < 0.05$.

Analytical solutions to eq 44 quickly become intractable for more than two sites. For fast exchange in a linear three-site model, represented by

$$A_3 \underset{k_{13}}{\overset{k_{31}}{\rightleftharpoons}} A_1 \underset{k_{21}}{\overset{k_{12}}{\rightleftharpoons}} A_2 \quad (52)$$

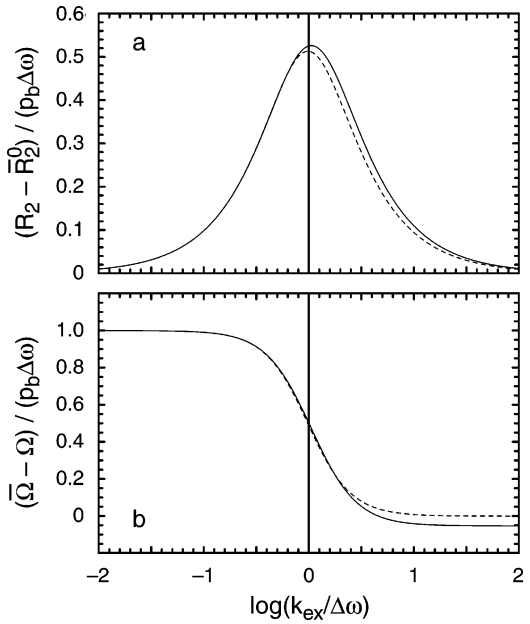

Figure 9. (a) Exchange-broadened transverse relaxation rate constant is shown for (—) the approximation of eq 50 and (- – -) the exact expression, eq 47 for $p_1 = 0.95$. (b) Resonance offset for two-site chemical exchange constants is shown for (—) the approximation of eq 51 and (- – -) the exact expression, eq 48 for $p_1 = 0.95$.

the relaxation rate constant is given by eq 44 with[108]

$$\langle u_1|\omega|u_2\rangle^2 = (-\kappa_3\alpha_1 + \alpha_2)/Z$$
$$\langle u_1|\omega|u_3\rangle^2 = (-\kappa_2\alpha_1 + \alpha_2)/Z$$
$$\kappa_2 = (k_{ex} + Z)/2$$
$$\kappa_3 = (k_{ex} - Z)/2 \qquad (53)$$

in which

$$k_{ex} = k_{12} + k_{21} + k_{13} + k_{31}$$
$$Z = (k_{ex}^2 - 4B)^{1/2}$$
$$B = k_{21}k_{31} + k_{12}k_{31} + k_{21}k_{13}$$
$$\alpha_1 = p_1p_2(\Omega_2 - \Omega_1)^2 + p_2p_3(\Omega_3 - \Omega_2)^2 + p_1p_3(\Omega_3 - \Omega_1)^2$$
$$\alpha_2 = p_1[k_{12}(\Omega_2 - \Omega_1)^2 + k_{13}(\Omega_3 - \Omega_1)^2]$$
$$p_1 = k_{21}k_{31}/B$$
$$p_2 = k_{12}k_{31}/B$$
$$p_3 = k_{21}k_{13}/B \qquad (54)$$

Numerical solutions to the Bloch−McConnell equations are necessary for other reaction schemes or for relaxation outside of the fast exchange limit.[104]

Slow chemical exchange processes can be studied by monitoring the exchange of longitudinal magnetization between sites if the population of the minor sites are large enough to generate observable resonance signals.[48] The evolution of longitudinal magnetization is given simply by

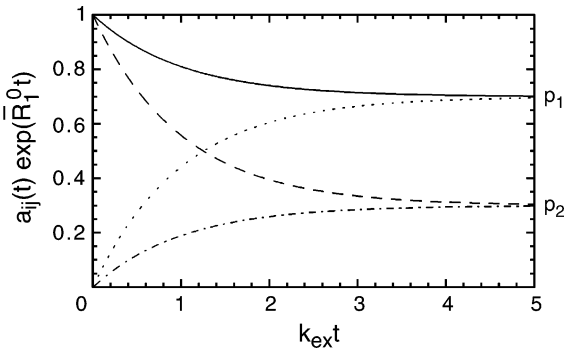

Figure 10. Population transfer due to chemical exchange. The transfer function amplitudes (—) $a_{11}(t)$, (– –) $a_{22}(t)$, (• • •) $a_{12}(t)$, and (- • -) $a_{21}(t)$ calculated using eq 57 are shown.

$$\Delta\mathbf{M}_z(t) = \exp[(-\rho_1 + \Gamma)t]\Delta\mathbf{M}_z(0) \qquad (55)$$

in which $\rho_{1jk} = \delta_{jk}R_{1k}^0$, $\Delta M_{zk}(t) = M_{zk}(t) - p_kM_z^{eq}$, and M_z^{eq} is the equilibrium longitudinal magnetization. For two site exchange, and assuming that $|\Delta R_{1k}^0| = |R_{1k}^0 - \bar{R}_1^0| \ll |\Gamma_{kk}|$

$$\begin{bmatrix}\Delta M_{z1}(t)\\ \Delta M_{z2}(t)\end{bmatrix} = \begin{bmatrix}a_{11}(t) & a_{12}(t)\\ a_{21}(t) & a_{22}(t)\end{bmatrix}\begin{bmatrix}\Delta M_{z1}(0)\\ \Delta M_{z2}(0)\end{bmatrix} \qquad (56)$$

in which

$$a_{11}(t) = [p_1 + p_2\exp(-k_{ex}t)]\exp(-\bar{R}_1^0 t)$$
$$a_{22}(t) = [p_2 + p_1\exp(-k_{ex}t)]\exp(-\bar{R}_1^0 t)$$
$$a_{12}(t) = p_1[(1 - \exp(-k_{ex}t))]\exp(-\bar{R}_1^0 t)$$
$$a_{21}(t) = p_2[(1 - \exp(-k_{ex}t))]\exp(-\bar{R}_1^0 t) \qquad (57)$$

The time dependence of $a_{ij}(t)$ is shown in Figure 10. As shown by eq 57, k_{ex} must not be much less than R_{1k}^0 for the exchanging sites; otherwise, the signals decay due to relaxation faster than population transfer.

3.3. Evolution in the Presence of rf Fields: $R_1\rho$ Relaxation

In an $R_{1\rho}$ experiment, magnetization is spin-locked in the rotating frame by application of a radio frequency field.[98,109] The relaxation rate constant for magnetization locked parallel to the effective field in the rotating reference frame is called $R_{1\rho}$. The dependence of the $R_1\rho$ relaxation rate constant on the amplitude or offset of the rf field is called relaxation dispersion.

In the limit of fast exchange, in which a single population-averaged resonance is observed, expressions for $R_{1\rho}$ are obtained by treating the changes in resonance frequencies resulting from transitions between sites as stochastic perturbations and utiliz-

ing Bloch−Wagness−Redfield theory. For n sites, the relaxation rate constant becomes[99]

$$R_{1\rho}(\omega_e) = \bar{R}_1^0 \cos^2\bar{\theta} + \bar{R}_2^0 \sin^2\bar{\theta} + \sin^2\bar{\theta}\sum_{k=2}^{n}\frac{\langle u_1|\omega|u_k\rangle^2}{\kappa_k}\left(\frac{\kappa_k^2}{\kappa_k^2 + \bar{\omega}_e^2}\right) \quad (58)$$

in which $\bar{\omega}_e = (\bar{\Omega}^2 + \omega_1^2)^{1/2}$, $\bar{\Omega}$ is the population-averaged resonance offset, and $\tan\bar{\theta} = \omega_1/\bar{\Omega}$. For two sites, this equation reduces to

$$R_{1\rho}(\omega_e) = \bar{R}_1^0 \cos^2\bar{\theta} + \bar{R}_2^0 \sin^2\bar{\theta} + \sin^2\bar{\theta}\left(\frac{p_1p_2\Delta\omega^2k_{ex}}{k_{ex}^2 + \bar{\omega}_e^2}\right) \quad (59)$$

Using eq 41, Trott and co-workers showed that the long-time evolution of the average magnetization in a $R_{1\rho}$ experiment can be approximated by[100,110]

$$\frac{d}{dt}\langle\mathbf{M}(t)\rangle = \mathbf{L}_0^{(1)}\langle\mathbf{M}(t)\rangle \quad (60)$$

in which

$$\mathbf{L}_0^{(1)} = [\mathbf{E} + p_1p_2\Delta(k_{ex} - \mathbf{C})^{-2}\Delta]^{-1} \times [\bar{\mathbf{L}} + p_1p_2\Delta(k_{ex} - \mathbf{C})^{-1}\Delta] \quad (61)$$

$$\bar{\mathbf{L}} = p_1\mathbf{L}_1 + p_2\mathbf{L}_2$$

$$\mathbf{C} = p_2\mathbf{L}_1 + p_1\mathbf{L}_2$$

$$\Delta = \mathbf{L}_2 - \mathbf{L}_1 \quad (62)$$

A general expression for the rotating-frame relaxation rate constant for site 1 ($p_1 > p_2$), $R_{1\rho}$, that encompasses all conformational exchange time scales is obtained from eq 61 by approximating the dominant eigenvalue of $\mathbf{L}_0^{(1)}$. The resulting expression, accurate whenever relaxation is dominated by a single-exponential decay, is given by

$$R_{1\rho} = \bar{R}_1^0 \cos^2\bar{\theta} + \bar{R}_2^0 \sin^2\bar{\theta} + \frac{1}{\gamma}\frac{\sin^2\theta p_1p_2\Delta\omega^2k_{ex}}{\omega_{e1}^2\omega_{e2}^2/\omega_e^2 + k_{ex}^2 - 2\sin^2\theta p_1p_2\Delta\omega^2 + (1-\gamma)\omega_1^2} \quad (63)$$

in which $\omega_{ek} = (\Omega_k^2 + \gamma\omega_1^2)^{1/2}$, $\omega_e = (\bar{\Omega}^2 + \gamma\omega_1^2)^{1/2}$, $\sin^2\theta = \gamma\omega_1^2/\omega_e^2$

$$\gamma = 1 + \frac{p_1p_2\Delta\omega^2(\sigma^2 + \omega_1^2 - k_{ex}^2)}{(\sigma^2 + \omega_1^2 + k_{ex}^2)^2} \quad (64)$$

and $\sigma = p_2\Omega_1 + p_1\Omega_2$. When $\gamma \to 1$, then $\omega_e \to \bar{\omega}_e$, and $\theta \to \bar{\theta}$. If the site populations are highly skewed ($p_1 \gg p_2$), then the simple result obtained is[110]

$$R_{1\rho} = \bar{R}_1\cos^2\bar{\theta} + \bar{R}_2\sin^2\bar{\theta} + \frac{\sin^2\bar{\theta}p_1p_2\Delta\omega^2k_{ex}}{\Omega_2^2 + \omega_1^2 + k_{ex}^2} \quad (65)$$

This expression has the same functional form as eq 59, except that the exchange contribution depends on the effective field for spins in the minor site 2, rather than on the effective field for the averaged resonance position. The accuracy of eqs 63 and 65 are illustrated in Figure 11.

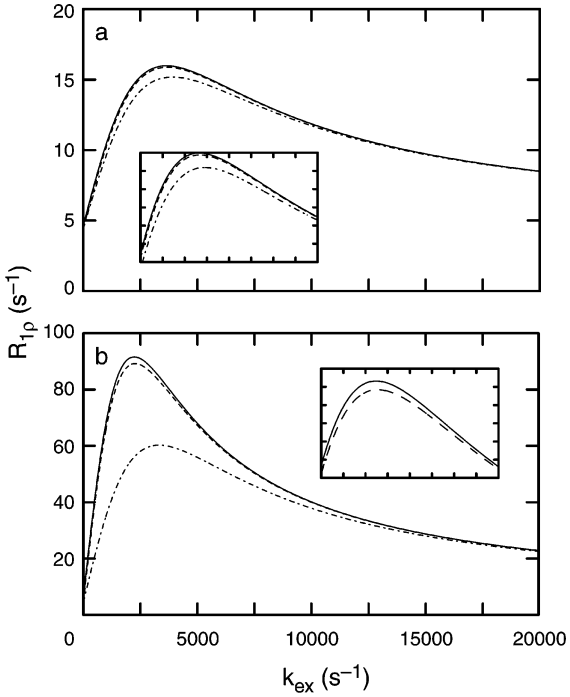

Figure 11. $R_{1\rho}$, for 2 site exchange. (—) Numerical solution to the 6 × 6 dimensional Bloch-McConnell equations. (- − -) Average magnetization approximation given by eq 63. (- • -) Approximate eigenvalue for highly skewed site populations given by eq 65. Results are shown for (a) $p_1 = 0.95$ and (b) $p_1 = 0.7$. Other parameters were $\Delta\omega = 2400$ s^{-1}, $\bar{\Omega} = 1500$ s^{-1}, $\omega_1 = 1000$ s^{-1}, $\bar{R}_1^0 = 1.5$ s^{-1}, and $\bar{R}_2^0 = 11$ s^{-1}. The insets show the regions (a) (1000, 10) to (9000, 16) and (b) (1000, 65) to (5000, 95).

As shown by comparison of eqs 59 and 65, slow to intermediate exchange exhibits a different dependence on the rf carrier frequency than does fast exchange in an $R_{1\rho}$, experiment. In particular, the exchange contribution to eq 59 has a maximum value for $\bar{\Omega} = 0$ and does not depend on the sign of $\bar{\Omega}$. In contrast, the exchange contribution to eq 65 has a maximum value for $\Omega_2^2 + \omega_1^2 = (\bar{\Omega} + p_1\Delta\omega)^2 + \omega_1^2 = 0$ and depends on the sign of $\bar{\Omega}$. These differences between fast and slow exchange in $R_{1\rho}$ relaxation have been confirmed experimentally.[111] The dependence of $R_{1\rho}$ on the tilt angle θ in eqs 58, 59, 63, and 65 can be removed by defining the pure exchange contribution to the relaxation rate constant as

$$R_{ex}(\omega_e) = R_{1\rho}/\sin^2\bar{\theta} - \bar{R}_2^0 - \bar{R}_1^0/\tan^2\bar{\theta} \quad (66)$$

Expressions for fast exchange relaxation rate constants for the three site linear model are obtained using eqs 53 and 54 in eq 58. The functional dependence of $R_{1\rho}$ on ω_e is shown in Figure 12.

3.4. Evolution during Spin–Echoes: CPMG Relaxation

In a CPMG experiment, the relaxation of transverse magnetization is observed during a (τ_{cp}/2−180°

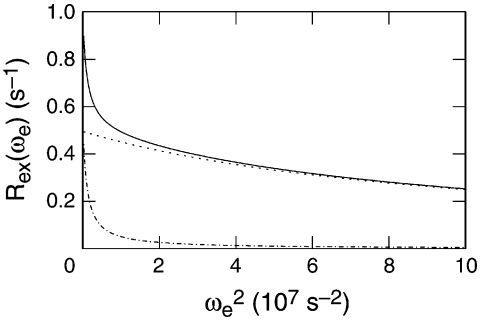

Figure 12. $R_{1\rho}$, for linear three-site exchange. (—) Theoretical dispersion curve generated using the fast-limit approximation, eq 58 (—) for $k_{12} = 10$ s^{-1}, $k_{21} = 1000$ s^{-1}, $k_{13} = 100$ s^{-1}, $k_{31} = 10\,000$ s^{-1}, $\Omega_1 = 0$ s^{-1}, $\Omega_2 = 250$ s^{-1}, and $\Omega_3 = 750$ s^{-1}. The curves are scaled relative to the value of R_{ex} for $\omega_e = 0$. Also shown are the dispersion profiles for the (- · -) $A_1 \leftrightarrow A_2$ and (···) $A_1 \leftrightarrow A_3$ transitions treated with independent two-site exchange models according to eq 59.

$-\tau_{cp} - 180°\text{-}\tau_{cp}/2)_n$ spin−echo sequence, in which τ_{cp} is the spacing between 180° pulses and n is an integer.[112,113] Evolution during a CPMG experiment can be analyzed by recognizing that the effect of the 180° pulse in the sequence, $\tau_{cp}/2-180°-\tau_{cp}/2$, is to invert the sense of precession of the nuclear spins. Under conditions for which the evolution of magnetization is dominated by a single-exponential decay, the transverse relaxation rate constant is given by[104]

$$R_2(1/\tau_{cp}) = \bar{R}_2^0 - \frac{1}{2\tau_{cp}} \ln \lambda$$

in which λ is the largest eigenvalue of the Hermetian matrix **A**

$$\mathbf{A} = \exp[(i\omega + \Gamma)\tau_{cp}] \exp[(i\omega + \Gamma)\tau_{cp}] \quad (67)$$

In the limit of fast exchange, in which a single population-averaged resonance is observed, the relaxation rate constant becomes

$$R_2(1/\tau_{cp}) = \bar{R}_2^0 + \sum_{k=2}^{n} \frac{\langle u_1|\omega|u_k\rangle^2}{\kappa_k}\left(1 - \frac{2\tanh[\kappa_k\tau_{cp}/2]}{\kappa_k\tau_{cp}}\right) \quad (68)$$

For 2 sites, this equation reduces to

$$R_2(1/\tau_{cp}) = \bar{R}_2^0 + \frac{p_1p_2\Delta\omega^2}{k_{ex}}\left(1 - \frac{2\tanh[k_{ex}\tau_{cp}/2]}{k_{ex}\tau_{cp}}\right) \quad (69)$$

A general expression for the transverse relaxation rate constant for site 1 ($p_1 > p_2$), $R_2(1/\tau_{cp})$, that encompasses all conformational exchange time scales is given by[98,114,115]

$$R_2(1/\tau_{cp}) = \bar{R}_2^0 + \frac{1}{2}\left(k_{ex} - \frac{1}{\tau_{cp}}\cosh^{-1}[D_+\cosh(\eta_+) - D_-\cos(\eta_-)]\right) \quad (70)$$

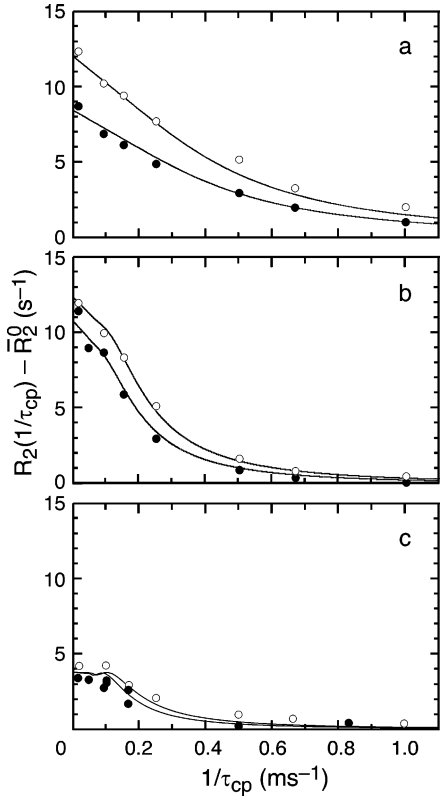

Figure 13. CPMG relaxation dispersion for Cys 38 in basic pancreatic trypsin inhibitor at (a) 313, (b) 300, and (c) 290 K. Values of $R_2(1/\tau_{cp})$ at (●) $\mathbf{B}_0 = 11.7$ T and (○) $\mathbf{B}_0 = 14.1$ T are shown at each temperature. In part a, the lines are the best simultaneous fit of eq 69 to data recorded at $\mathbf{B}_0 = 11.7$ and 14.1 T; in parts b and c, the lines are the best simultaneous fit of eq 70. Exchange is fast at 313 K, intermediate at 300 K and slow at 290 K.

in which

$$D_\pm = \frac{1}{2}\left[\pm 1 + \frac{\psi + 2\Delta\omega^2}{(\psi^2 + \zeta^2)^{1/2}}\right]^{1/2}$$

$$\eta_\pm = \frac{\tau_{cp}}{2}[\pm\psi + (\psi^2 + \zeta^2)^{1/2}]^{1/2} \quad (71)$$

$\psi = k_{ex}^2 + \Delta\omega^2$ and $\zeta = -2\Delta\omega k_{ex}(p_1 - p_2)$. CPMG relaxation dispersion for fast and slow exchange is illustrated in Figure 13.

Expressions for fast exchange relaxation rate constants for the three site linear model are obtained using eqs 53 and 54 in eq 68. The functional dependence of $R_2(1/\tau_{cp})$ on $1/\tau_{cp}$ is shown in Figure 14.

3.5. Chemical Exchange in Multiple Quantum Spectroscopy

If two spins are affected by the same chemical exchange kinetic process, then the chemical shift changes for the two spins resulting from transitions between sites will be correlated. This correlation gives rise to exchange effects that can either broaden or narrow resonance line shapes for multiple quantum coherences.[116] For simplicity, only two-site exchange is considered; extension to more than two sites is straightforward. For multiple quantum coherences, the value of $\Delta\omega$ in the equations given above should be replaced by the difference in multiple

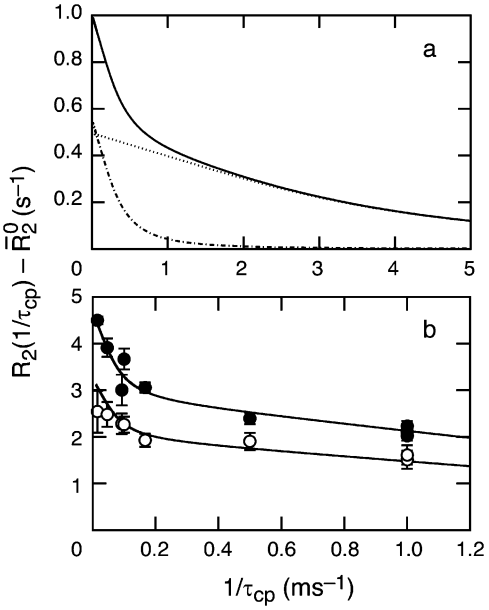

Figure 14. $R_2(1/\tau_{cp})$ for linear three-site exchange. (a) (—) Theoretical dispersion curve generated using the fast-limit approximation, eq 68 (—) for $k_{12} = 10$ s^{-1}, $k_{21} = 1000$ s^{-1}, $k_{13} = 100$ s^{-1}, $k_{31} = 10\,000$ s^{-1}, $\Omega_1 = 0$ s^{-1}, $\Omega_2 = 250$ s^{-1}, and $\Omega_3 = 750$ s^{-1}. The curves are scaled relative to the value of $R_2(1/\tau_{cp}) - \bar{R}_2^0$ for $1/\tau_{cp} = 0$. Also shown are the dispersion profiles for the (- · -) $A_1 \leftrightarrow A_2$ and (···) $A_1 \leftrightarrow A_3$ transitions treated with independent two-site exchange models according to eq 69. (b) ^{15}N R_{ex} ($/\tau_{cp}$) relaxation dispersion profiles for Cys14 in basic pancreatic trypsin inhibitor at 300 K and static magnetic field strengths of 11.7 (○) and 14.1 T (●). The solid lines represent the best simultaneous fit of the data at both static magnetic fields to the linear three-site model. Reproduced with permission from ref 108. Copyright 2003 Am. Chem. Soc.

quantum frequencies, $\Delta\omega_{MQ}$. For I^+S^+ double (DQ) and $I-S^+$ zero (ZQ) quantum coherences, respectively, $\Delta\omega_{DQ} = \Delta\omega_I + \Delta\omega_S$ and $\Delta\omega_{ZQ} = -\Delta\omega_I + \Delta\omega_S$, in which $\Delta\omega_I$ ($\Delta\omega_S$) is the chemical shift difference between sites 1 and 2 for the I (S) spin.

Using eq 50, applicable when $p_1 \gg p_2$, the difference in relaxation rate constants for DQ and ZQ coherence is given by[117]

$$\Delta R_{MQ} = R_{ZQ} - R_{DQ} = \bar{R}_{ZQ}^0 - \bar{R}_{DQ}^0 + \frac{4p_1^2 p_2 \Delta\omega_I \Delta\omega_S k_{ex}^3}{p_1^4 k_{ex}^4 + 2p_1^2 k_{ex}^2(\Delta\omega_I^2 + \Delta\omega_S^2) + (\Delta\omega_I^2 - \Delta\omega_S^2)^2} \quad (72)$$

The difference $\bar{R}_{ZQ}^0 - \bar{R}_{DQ}^0$ is small; consequently, the sign of ΔR_{MQ} gives the relative sign of the chemical shift differences for I and S spins.[118] This information, which cannot be obtained from single quantum experiments, is helpful for mechanistic interpretations of exchange phenomena. Multiple quantum analogues of the single quantum CPMG experiment have begun to be utilized in studies of protein conformational dynamics.[119−121]

For a heteronuclear spin system (S = ^{15}N or ^{13}C and I = ^{1}H), the HMQC experiment records the average of the DQ and ZQ evolution frequencies, whereas the HSQC experiment records the single quantum frequency. Using eq 51, applicable when $p_1 \gg p_2$, the difference between the frequencies recorded in the HSQC and HMQC experiments is given by[122]

$$\Delta\Omega = \Omega_{HSQC} - \Omega_{HMQC} = \left[\frac{p_1 p_2 \Delta\omega_S \Delta\omega_I^2 k_{ex}^2}{p_1^2 k_{ex}^2 + \Delta\omega_S^2}\right] \times \left[\frac{3p_1^2 k_{ex}^2 + \Delta\omega_I^2 - \Delta\omega_S^2}{p_1^4 k_{ex}^4 + 2p_1^2 k_{ex}^2(\Delta\omega_I^2 + \Delta\omega_S^2) + (\Delta\omega_I^2 - \Delta\omega_S^2)^2}\right] \quad (73)$$

As shown by Skrynnikov and co-workers,[122] the second bracketed term is positive for a wide range of applicable parameters and therefore the sign of $\Delta\Omega$ is the same as the sign of $\Delta\omega_S$. Thus, provided that exchange is not in the fast limit, the sign of $\Delta\omega_S$ can be determined simply by comparing HSQC and HMQC spectra. Examples of ΔR_{MQ} and $\Delta\Omega$ measured for basic pancreatic trypsin inhibitor are shown in Figure 15.

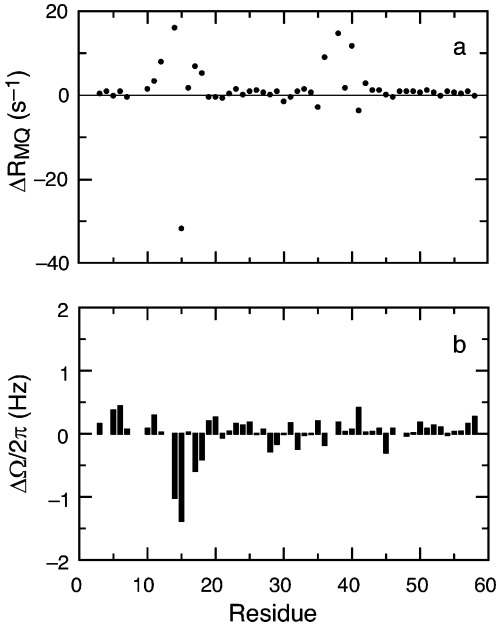

Figure 15. ^{15}N-^{1}H multiple quantum relaxation in basic pancreatic trypsin inhibitor. (a) ΔR_{MQ} measured at 14.1 T and 300 K.[117] Prominent exchange broadening is evident in the vicinity of the Cys 14-Cys 38 disulfide bond. The negative value of ΔR_{MQ} for Lys 15 indicates that $\Delta\omega_N$ and $\Delta\omega_H$ have opposite signs. (b) $\Delta\Omega$ determined from HSQC and HMQC experiments recorded at 11.7 T and 280 K.[108] The negative values of $\Delta\Omega$ for Cys 14 and Lys 15 indicate that $\Delta\omega_N$ is negative for these two residues.

3.6. Interpretation of Chemical Exchange Processes

Experimental techniques described above enable chemical exchange constants to be determined over a range from 0.1 to 10^5 s^{-1} using ZZ exchange, line shape, CPMG, and $R_{1\rho}$ methods. Data analysis normally involves fitting appropriate theoretical expressions, given above, to time series, frequency domain spectra, and relaxation dispersion curves. As indicated by eqs 49 and 53, in the fast exchange limit, site populations cannot be determined independently of the squares of the chemical shift differences (Ω_j −

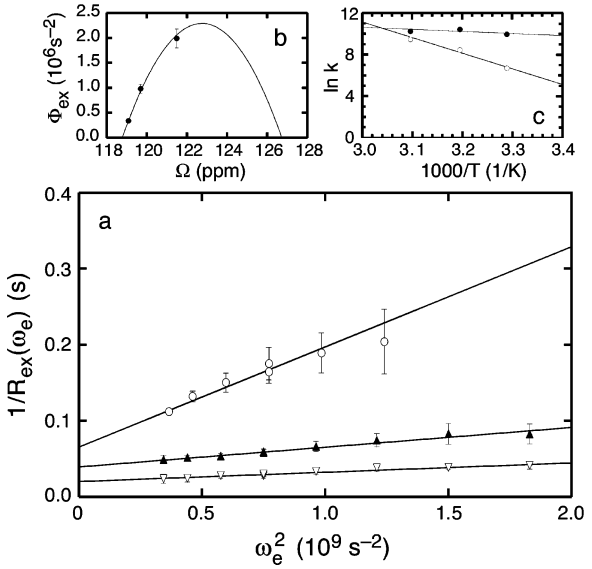

Figure 16. ^{15}N $R_{1\rho}$ relaxation dispersion for Ala 11 of PSBD.[126] (a) Data recorded at 304 (○), 313 (▲), and 323 K (▽). R_{ex} data for Ala 11 were obtained from eq 66. The best least-squares fitted line is drawn for each data set. (b) $\Phi_{ex} = p_1p_2\Delta\omega$ is plotted versus the isotropic shift Ω at each temperature. The solid line is the best fit to determine the x intercepts $\Omega_1 = 118.80 \pm 0.02$ ppm and $\Omega_2 = 126.7 \pm 0.4$ ppm with $\Delta\omega = 7.9 \pm 0.4$ ppm. The chemical shift of the (unobserved) unfolded PSBD species is in good agreement with the predicted random coil chemical shift of 126.0 ppm for an Ala residue preceded by a Tyr residue.[212] (c) Arrhenius plot for (●) folding (k_{-1}) and (○) unfolding (k_1) rate constants. The apparent activation barriers are 17 ± 14 kJ mol^{-1} for folding and 125 ± 19 kJ mol^{-1} for unfolding.

$\Omega_k)^2$. Outside of the fast exchange limit, site populations and the absolute sign of $\Omega_j - \Omega_k$ potentially can be determined independently.[110,122] Thus, manipulation of the time scale of chemical exchange by varying the temperature, pH, or ligand concentration facilitates complete analysis of the exchange parameters.[108,123,124] Furthermore, the field dependence of exchange broadening provides information on the exchange time scale and increases the reliability of curve-fitting through global data analysis.[125] Data analysis is facilitated if R_2^0 is known independently, rather than being treated as an adjustable parameter during curve-fitting; methods for determining R_2^0 have been reviewed.[42]

The temperature dependence of chemical exchange parameters can be analyzed to determine apparent Arrhenius and Boltzmann parameters for activation barriers and energetic differences between sites. An example of such an analysis is illustrated in Figure 16 for the peripheral subunit binding domain (PSBD) from the dihydrolopoamide acetyltransferase component of the pyruvate dehydrogenase multienzyme complex from *Bacillus stearothermophilus*.[126] The exchange process arising from the equilibrium unfolding of the molecule was characterized using ^{15}N $R_{1\rho}$ measurements. The relaxation dispersion curve was linearized by plotting $1/R_{ex}(\omega_e)$ versus ω_e^2, as shown in Figure 16a. In the fast-exchange limit, only values of k_{ex} and $\Phi_{ex} = p_1p_2\Delta\omega^2$ are obtained from the data analysis at each temperature. Values of Ω_1 and Ω_2, and hence $\Delta\omega$, can be obtained from the temperature dependence of $\bar{\Omega}$ and Φ_{ex}, because Φ_{ex}

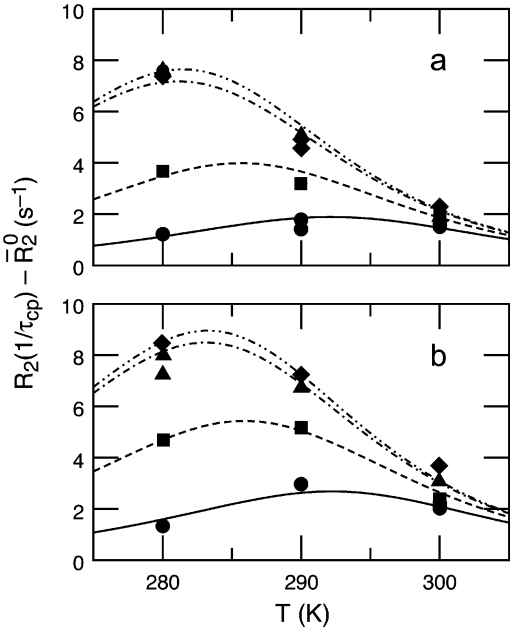

Figure 17. Global analysis of the temperature dependence of chemical exchange for Cys 14. ^{15}N $R_2(1/\tau_{cp})$ relaxation rate constants for Cys 14 at static magnetic field strengths of (a) 11.7 and (b) 14.1 T and temperatures of 300, 290, and 280 K were measured for τ_{cp} = 1 (●, —), 2 (■, - - -), 6 (▲, - · -) and 10 ms (◆, - ·· -). The lines represent the global fit of the dispersion data at both fields and the three temperatures to eqs 69 and 70 expressed as a function of temperature by optimization of the activation parameters and $\Delta\omega$ for the exchange kinetic process. Reproduced with permission from ref 108. Copyright 2003 Am. Chem. Soc.

$= -\bar{\Omega}^2 + (\Omega_1 + \Omega_2) - \Omega_1\Omega_2$. Once $\Delta\omega$ is known, p_1, p_2, k_{12}, and k_{21} are obtained from Φ_{ex} and k_{ex} at each temperature.

An additional example is shown in Figure 17. A global analysis of CPMG relaxation dispersion at three temperatures and two static magnetic fields was performed for Cys 14 in BPTI.[108] At 290 K, the exchange process occurs with forward and reverse rate constants of 35 and 2500 s^{-1}, respectively, and the minor state conformation is populated by 1.4% of the molecules at equilibrium. The absolute value of $\Delta\omega$ was determined from the global analysis and the sign of $\Delta\omega$ was obtained from comparing HSQC and HMQC spectra, as shown in Figure 15. The chemical shift information was used to develop a model for the unknown minor conformational state by both inspection of a chemical shift database[127] and calculation of chemical shifts using the SHIFTX program.[128] The agreement between calculated and experimental shifts suggests that the exchange processes results from rotamer transitions of the Cys 14 χ_1 dihedral angle.[108]

4. Applications to Proteins and Other Biological Macromolecules

The first global analysis of protein dynamics by modern NMR spin relaxation methods was reported in 1989. By 1997, the number of applications to proteins, nucleic acids, and other biological macromolecules already had grown too large to be individually cited in review articles.[2] In 2004, the use of spin relaxation techniques to investigate conforma-

tional dynamics in biological molecules has become a standard approach in structural biology. The approaches described above have been extensively applied to investigate ligand binding and chemical modifications, enzyme catalysis, and folding. The large majority of applications are to proteins; however, applications to nucleic acids[129−133] and oligosaccharides[134−137] are increasing. Selected applications in these areas are presented below.

4.1. Ligand Binding and Chemical Modifications

Spin relaxation has been used in a number of systems to investigate ligand binding and chemical modifications, such as changes in redox[138−140] or phosphorylation state.[141,142] Both ps−ns and μs−ms time scale processes have been of interest in these studies. Equations 28 and 27 suggest that changes in configurational entropy resulting from changes in intramolecular dynamics on multiple time scales may contribute significantly to protein thermodynamics. Chemical exchange line broadening in the apo or unmodified states of proteins may reflect kinetic transitions between active (competent) and inactive (uncompetent) conformations within an ensemble of states. Chemical exchange line broadening in ligated states may reflect binding kinetics and conformational transitions associated with gating of ligand into protein active sites.[143,144] Although a large number of studies have been reported in the literature, a smaller number of systems have been the subject of extensive investigation with multiple techniques, homologues or mutants, and ligands. These systems include, adenylate kinase;[52,145−147] calmodulin and other calcium-binding proteins, such as calbindin D_{9k},[76,148,149] S100B,[150] and troponin C;[151−153] fatty acid binding proteins;[154−159] HIV-1 protease;[160−163] a cavity mutant of T4 lysozyme;[144,164−167] and SH2 domains.[168−171]

Applications in which conformational entropy is deduced from changes in generalized order parameters present a complex picture in which both increases[76,172−174] and decreases[175,176] in rigidity are observed for protein−ligand interactions; in addition, substantial differences in the response to ligand binding can be observed between backbone and side chain probes of conformational flexibility.[172] In some cases, important correlations between changes in flexibility and calorimetric measurements of the entropy of binding or equilibrium affinity constants have been elucidated.[172−174] Substantial questions remain concerning how information for multiple probes (^{13}CO and ^{15}N, for example) should be combined,[22,177,178] how side chain and backbone studies should be integrated,[179] and how site-to-site correlations between dynamic processes affecting individual spins should be handled.[74]

Measurements of chemical exchange broadening increasingly are being used to support models for ligand-binding or conformational changes in which binding or modification selects compenent conformations from a preexisting ensemble.[141,142,180] Thus, at equilibrium in the apo or unmodified state, individual molecules fluctuate stochastically between active and inactive conformations. Binding of ligand or chemical modification shifts the equilibrium increasingly toward the active conformation. Observation of similar kinetic rates for intramolecular conformational changes and ligand binding provide suggestive evidence that conformational transitions are coupled to binding or release of ligand.[144] This emerging view is in contrast to both lock-and-key and induced fit models for ligand binding.[181]

4.2. Enzyme Catalysis

Elucidation of the dynamic properties of enzymes that are correlated with catalytic activity is an important goal of longstanding interest in NMR spectrocopy. Recent studies of adenylate kinase,[52,145−147] cyclophilin A,[123] dihydrofolate reductase (DHFR),[182,183] HIV-1 protease,[160−163] ribonucleases,[75,184] serine proteases,[185−187] and triosephosphate isomerase[188,189] have identified conformational exchange processes on picosecond−nanosecond and microsecond−millisecond time scales in enzyme active sites that may play roles in catalysis as well as substrate binding. Similar studies have begun to be applied to RNA ribozymes.[132] The information available from NMR spin relaxation studies about the effects of substrate binding and product release is similar to that discussed above for ligand binding. The dependence of the dynamic properties of the protein on ligand concentration can be used to distinguish contributions from substrate binding or product release and contributions from catalysis.[123] Investigations are facilitated if the enzyme system has been highly characterized biochemically, so that a well-developed kinetic mechanism exists and multiple substrate analogues, inhibitors, and transition state analogues are available. The large body of information available on adenylate kinase, DHFR, and HIV-1 protease exemplify these approaches. Most studies of enzymes to date have been performed on inhibited proteins or in the absence of substrates. In the case of cyclophilin A, however, measurements of exchange broadening were performed while the protein was actively turning over substrate.[123] Similar studies on other enzymes catalyzing reversible reactions, or for which regeneration systems can be developed, are likely to be extremely powerful in the future.

4.3. Protein Folding

Investigations of protein folding by NMR spin relaxation techniques have included measurements of protein folding kinetics and characterization of the ensemble of unfolded conformations. Although useful information can be obtained by monitoring resolved aromatic or methyl ^{1}H resonances in 1D NMR spectra, for example in line shape analysis of protein folding,[190,191] the use of isotopically labeled molecules allows the range of spin relaxation techniques to be applied with site specific resolution. These approaches are particularly important for unfolded or non-native states that frequently display reduced chemical shift dispersion.[192]

Kinetics of protein folding have been investigated by techniques based on chemical exchange phenom-

ena, including zz-exchange spectroscopy,[193,194] line shape analysis,[190,191] CPMG dispersion,[194,195] and $R_{1\rho}$ dispersion.[126] Notably, the choice of experimental technique can be made based on the time scale of folding. As illustrated for PSBD, values of $\Delta\omega$ derived from the analysis of chemical exchange provide unique information about the unfolded ensemble of conformations at equilibrium under native state conditions.[126] Comparisons between folding rate constants for different sites in a protein, a particular strength of NMR techniques, potentially provides important insights into the mechanism of folding.[194,195] These experiments complement amide proton solvent exchange techniques for studying protein folding.[196]

Spin relaxation in unfolded or non-native proteins potentially is a powerful approach for characterizing the conformational ensemble of thermally accessible states. Because an ensemble of structures with unique overall and internal motions contributes to the observed relaxation parameters, the interpretation of experimental results is correspondingly more complex than for compact globular proteins; consequently, in addition to spectral density mapping and model free approaches, methods based on distributions of correlation times have been utilized to analyze relaxation data.[53,54] Computational simulations are essential in augmenting and interpreting experimental results.[197] Myoglobin,[198−201] SH3 domains,[194,202−204] and staphylococcal nuclease[205−208] have been extensively studied by spin relaxation techniques. A general result is that, under unfolding conditions, the residual structure in some regions of the polypeptide chain and (partially) collapsed states can be identified by spin relaxation measurements. Relaxation studies of non-native states have been complemented recently by investigations of residual dipolar couplings.[209]

The possible contribution of conformational dynamics to the thermodynamics of protein folding has attracted interest, both because a large change in heat capacity is observed for proteins upon folding and because theoretical estimates suggest substantial loss of conformational entropy in the native folded state. The contributions of backbone entropy to thermodynamic stability in protein G B1 domain has been inferred by comparison of generalized order parameters in a series of site specific mutant proteins.[210] The temperature dependence of the generalized order parameter also has been used to estimate heat capacity changes resulting from folding.[79,179]

5. Conclusion

Over the past 15 years, the experimental and theoretical methods for analyzing molecular dynamics by NMR spin relaxation spectroscopy have grown inexorably more powerful. Applications of these methods have expanded to encompass investigations of conformational dynamics on multiple time scales for diverse functional states of biological macromolecules in order to characterize folding, stability, and biological activity. Continued development and application of NMR spin relaxation techniques promise to enhance understanding of the biological functions of proteins, nucleic acids, and other biological macromolecules.

6. Acknowledgments

A.G.P. is grateful to Joel Butterwick, Michael Grey, Francesca Massi, and Chunyu Wang (Columbia University) for helpful discussions and assistance with figures. This work was supported by Grants GM50291 and GM59273 from the National Institutes of Health.

7. References

(1) Palmer, A. G.; Williams, J.; McDermott, A. *J. Phys. Chem.* **1996**, *100*, 13293.
(2) Palmer, A. G. *Curr. Opin. Struct. Biol.* **1997**, *7*, 732.
(3) Palmer, A. G.; Kroenke, C. D.; Loria, J. P. *Methods Enzymol.* **2001**, *204−238*, 204.
(4) Fischer, M. W. F.; Majumdar, A.; Zuiderweg, E. R. P. *Prog. Nucl. Magn. Reson. Spectrosc.* **1998**, *33*, 207.
(5) Luginbuhl, P.; Wüthrich, K. *Prog. Nucl. Magn. Reson. Spectrosc.* **2002**, *40*, 199.
(6) Goldman, M. *J. Magn. Res.* **2001**, *149*, 160.
(7) Murali, N.; Krishnan, V. V. *Concepts Magn. Reson.* **2003**, *17A*, 86.
(8) Hernandez, G.; LeMaster, D. M. *Biochemistry* **2001**, *40*, 14384.
(9) Hernandez, G.; Jenney, F. E., Jr.; Adams, M. W. W.; LeMaster, D. M. *Proc. Nat. Acad. Sci. U.S.A.* **2000**, *97*, 3166.
(10) Chou, J. J.; Case, D. A.; Bax, A. *J. Am. Chem. Soc.* **2003**, *125*, 8959.
(11) Tolman, J. R. *J. Am. Chem. Soc.* **2002**, *124*, 12020.
(12) Meiler, J.; Peti, W.; Griesinger, C. *J. Am. Chem. Soc.* **2003**, *125*, 8072.
(13) Lukin, J. A.; Kontaxis, G.; Simplaceanu, V.; Yuan, Y.; Bax, A.; Ho, C. *Proc. Nat. Acad. Sci. U.S.A.* **2003**, *100*, 517.
(14) Peti, W.; Meiler, J.; Brüschweiler, R.; Griesinger, C. *J. Am. Chem. Soc.* **2002**, *124*, 5822.
(15) Al-Hashimi, H. M.; Goser, Y.; Gorin, A.; Hu, W.; Majumdar, A.; Patel, D. J. *J. Mol. Biol.* **2002**, *315*, 95.
(16) Briggman, K. B.; Tolman, J. R. *J. Am. Chem. Soc.* **2003**, *125*, 10164.
(17) Clore, G. M.; Schwieters, C. D. *J. Am. Chem. Soc.* **2004**, *126*, 2923.
(18) Cavanagh, J.; Fairbrother, W. J.; Palmer, A. G.; Skelton, N. J. *Protein NMR Spectroscopy: Principles and practice*; Academic Press: San Diego, CA, 1996.
(19) Kay, L. E.; Torchia, D. A.; Bax, A. *Biochemistry* **1989**, *28*, 8972.
(20) Millet, O.; Muhandiram, D. R.; Skrynnikov, N. R.; Kay, L. E. *J. Am. Chem. Soc.* **2002**, *124*, 6439.
(21) Skrynnikov, N. R.; Millet, O.; Kay, L. E. *J. Am. Chem. Soc.* **2002**, *124*, 6449.
(22) Wang, T.; Cai, S.; Zuiderweg, E. R. P. *J. Am. Chem. Soc.* **2003**, *125*, 8639.
(23) Abragam, A. *Principles of Nuclear Magnetism*; Clarendon Press: Oxford, U.K., 1961.
(24) Fushman, D.; Cowburn, D. *J. Biomol. NMR* **1999**, *13*, 139.
(25) Boyd, J.; Redfield, C. *J. Am. Chem. Soc.* **1998**, *120*, 9692.
(26) Case, D. A. *J. Biomol. NMR* **1999**, *15*, 95.
(27) Ottiger, M.; Bax, A. *J. Am. Chem. Soc.* **1998**, *120*, 12334.
(28) Boyd, J.; Redfield, C. *J. Am. Chem. Soc.* **1999**, *121*, 7441.
(29) Fushman, D.; Tjandra, N.; Cowburn, D. *J. Am. Chem. Soc.* **1998**, *120*, 10947.
(30) Kroenke, C. D.; Rance, M.; Palmer, A. G. *J. Am. Chem. Soc.* **1999**, *121*, 10119.
(31) Scheurer, C.; Skrynnikov, N. R.; Lienin, S. F.; Straus, S. K.; Brüschweiler, R.; Ernst, R. R. *J. Am. Chem. Soc.* **1999**, *121*, 4242.
(32) Tjandra, N.; Szabo, A.; Bax, A. *J. Am. Chem. Soc.* **1996**, *118*, 6986.
(33) Mittermaier, A.; Kay, L. E. *J. Am. Chem. Soc.* **1999**, *121*, 10608.
(34) Mandel, A. M.; Akke, M.; Palmer, A. G. *J. Mol. Biol.* **1995**, *246*, 144.
(35) Peng, J. W.; Wagner, G. *J. Magn. Reson.* **1992**, *98*, 308.
(36) Peng, J. W.; Wagner, G. *Biochemistry* **1992**, *31*, 8571.
(37) Farrow, N. A.; Zhang, O.; Szabo, A.; Torchia, D. A.; Kay, L. E. *J. Biomol. NMR* **1995**, *6*, 153.
(38) Ishima, R.; Nagayama, K. *J. Magn. Reson., Ser. B* **1995**, *108*, 73.
(39) Ishima, R.; Nagayama, K. *Biochemistry* **1995**, *34*, 3162.
(40) Peng, J. W.; Wagner, G. *Biochemistry* **1995**, *34*, 16733.
(41) Phan, I. Q. H.; Boyd, J.; Campbell, I. D. *J. Biomol. NMR* **1996**, *8*, 369.
(42) Wang, C.; Palmer, A. G. *Magn. Reson. Chem.* **2003**, *41*, 866.

(43) Clore, G. M.; Szabo, A.; Bax, A.; Kay, L. E.; Driscoll, P. C.; Gronenborn, A. M. *J. Am. Chem. Soc.* **1990**, *112*, 4989.
(44) Lipari, G.; Szabo, A. *J. Am. Chem. Soc.* **1982**, *104*, 4546.
(45) Lipari, G.; Szabo, A. *J. Am. Chem. Soc.* **1982**, *104*, 4559.
(46) Mayo, K. H.; Daragan, V. A.; Idiyatullin, D.; Nesmelova, I. *J. Magn. Reson.* **2000**, *146*, 188.
(47) Brüschweiler, R.; Case, D. A. *Phys. Rev. Lett.* **1994**, *72*, 940.
(48) Led, J. J.; Gesmar, H.; Abildgaard, F. *Methods Enzymol.* **1989**, *176*, 311.
(49) LeMaster, D. M. *J. Am. Chem. Soc.* **1999**, *121*, 1726.
(50) Lienin, S. F.; Bremi, T.; Brutscher, B.; Brüschweiler, R.; Ernst, R. R. *J. Am. Chem. Soc.* **1998**, *120*, 9870.
(51) Meirovitch, E.; Shapiro, Y. E.; Liang, Z.; Freed, J. H. *J. Phys. Chem. B* **2003**, *107*, 9898.
(52) Tugarinov, V.; Liang, Z.; Shapiro, Y. E.; Freed, J. H.; Meirovitch, E. *J. Am. Chem. Soc.* **2001**, *123*, 3055.
(53) Buevich, A. V.; Baum, J. *J. Am. Chem. Soc.* **1999**, *121*, 8671.
(54) Ochsenbein, F.; Neumann, J.-M.; Guittet, E.; Van Heijenoort, C. *Protein Sci.* **2002**, *11*, 957.
(55) Halle, B.; Wennerström, H. *J. Chem. Phys.* **1981**, *75*, 1928.
(56) Schurr, J. M.; Babcock, H. P.; Fujimoto, B. S. *J. Magn. Reson., Ser. B* **1994**, *105*, 211.
(57) Brüschweiler, R.; Liao, X.; Wright, P. E. *Science* **1995**, *268*, 886.
(58) Copié, V.; Tomita, Y.; Akiyama, S. K.; Aota, S.; Yamada, K. M.; Venable, R. M.; Pastor, R. W.; Krueger, S.; Torchia, D. A. *J. Mol. Biol.* **1998**, *277*, 663.
(59) Lee, L. K.; Rance, M.; Chazin, W. J.; Palmer, A. G. *J. Biomol. NMR* **1997**, *9*, 287.
(60) Fushman, D.; Xu, R.; Cowburn, D. *Biochemistry* **1999**, *38*, 10225.
(61) Andrec, M.; Montelione, G. T.; Levy, R. M. *J. Magn. Reson.* **1999**, *139*, 408.
(62) d'Auvergne, E. J.; Gooley, P. R. *J. Biomol. NMR* **2003**, *25*, 25.
(63) McMahon, M. T.; Oldfield, E. *J. Biomol. NMR* **1999**, *13*, 133.
(64) Palmer, A. G.; Rance, M.; Wright, P. E. *J. Am. Chem. Soc.* **1991**, *113*, 4371.
(65) Korzhnev, D. M.; Orekov, V. Y.; Arseniev, A. S. *J. Magn. Res.* **1997**, *127*, 184.
(66) Bremi, T.; Brüschweiler, R. *J. Am. Chem. Soc.* **1977**, *119*, 6672.
(67) Brüschweiler, R.; Wright, P. E. *J. Am. Chem. Soc.* **1994**, *116*, 8426.
(68) Goodman, J. L.; Pagel, M. D.; Stone, M. J. *J. Mol. Biol.* **2000**, *295*, 963.
(69) Zhang, F.; Brüschweiler, R. *J. Am. Chem. Soc.* **2002**, *124*, 12654.
(70) Mayer, K. L.; Earley, M. R.; Gupta, S.; Pichumani, K.; Regan, L.; Stone, M. J. *Nat. Struct. Biol.* **2003**, *10*, 962.
(71) Akke, M.; Brüschweiler, R.; Palmer, A. G. *J. Am. Chem. Soc.* **1993**, *115*, 9832.
(72) Li, Z.; Raychaudhuri, S.; Wand, A. J. *Protein Sci.* **1996**, *5*, 2647.
(73) Yang, D.; Kay, L. E. *J. Mol. Biol.* **1996**, *263*, 369.
(74) Prompers, J. J.; Brüschweiler, R. *J. Phys. Chem. B* **2000**, *104*, 11416.
(75) Wang, L. C.; Pang, Y. X.; Holder, T.; Brender, J. R.; Kurochkin, A. V.; Zuiderweg, E. R. P. *Proc. Nat. Acad. Sci. U.S.A.* **2001**, *98*, 7684.
(76) Akke, M.; Skelton, N. J.; Kördel, J.; Palmer, A. G.; Chazin, W. J. *Biochemistry* **1993**, *32*, 9832.
(77) Lee, A. L.; Sharp, K. A.; Kranz, J. K.; Song, X.-J.; Wand, A. J. *Biochemistry* **2002**, *41*, 13814.
(78) Mandel, A. M.; Akke, M.; Palmer, A. G. *Biochemistry* **1996**, *35*, 16009.
(79) Yang, D.; Mok, Y. K.; Forman-Kay, J. D.; Farrow, N. A.; Kay, L. E. *J. Mol. Biol.* **1997**, *272*, 790.
(80) Vugmeyster, L.; Trott, O.; James McKnight, C.; Raleigh, D. P.; Palmer, A. G. *J. Mol. Biol.* **2002**, *320*, 841.
(81) Massi, F.; Palmer, A. G. *J. Am. Chem. Soc.* **2003**, *125*, 11158.
(82) Seewald, M. J.; Pichumani, K.; Stowell, C.; Tibbals, B. V.; Regan, L.; Stone, M. J. *Protein Sci.* **2000**, *9*, 1177.
(83) Idiyatullin, D.; Nesmelova, I.; Daragan, V. A.; Mayo, K. H. *J. Mol. Biol.* **2003**, *325*, 149.
(84) Lee, A. L.; Wand, A. J. *Nature* **2001**, *411*, 501.
(85) Altieri, A. S.; Hinton, D. P.; Byrd, R. A. *J. Am. Chem. Soc.* **1995**, *117*, 7566.
(86) Bernado, P.; Garcia de la Torre, J.; Pons, M. *J. Biomol. NMR* **2002**, *23*, 139.
(87) Garcia de la Torre, J.; Huertas, M. L.; Carrasco, B. *J. Magn. Res.* **2000**, *147*, 138.
(88) Tjandra, N.; Garrett, D. S.; Gronenborn, A. M.; Bax, A.; Clore, G. M. *Nat. Struct. Biol.* **1997**, *4*, 443.
(89) Ulmer, T. S.; Werner, J. M.; Campbell, I. D. *Structure* **2002**, *10*, 901.
(90) Hwang, P. M.; Skrynnikov, N. R.; Kay, L. E. *J. Biomol. NMR* **2001**, *20*, 83.
(91) Ghose, R.; Fushman, D.; Cowburn, D. *J. Magn. Res.* **2001**, *149*, 204.
(92) Chang, S.-L.; Tjandra, N. *J. Am. Chem. Soc.* **2001**, *123*, 11484.
(93) Baber, J. L.; Szabo, A.; Tjandra, N. *J. Am. Chem. Soc.* **2001**, *123*, 3953.
(94) Chang, S.-L.; Szabo, A.; Tjandra, N. *J. Am. Chem. Soc.* **2003**, *125*, 11379.
(95) Goto, N. K.; Skrynnikov, N. R.; Dahlquist, F. W.; Kay, L. E. *J. Mol. Biol.* **2001**, *308*, 745.
(96) Fischer, M. W. F.; Losonczi, J. A.; Weaver, J. L.; Prestegard, J. H. *Biochemistry* **1999**, *38*, 9013.
(97) Sandstrom, J. *Dynamic NMR Spectroscopy*; Academic Press: London, 1982.
(98) Davis, D. G.; Perlman, M. E.; London, R. E. *J. Magn. Reson., Ser. B* **1994**, *104*, 266.
(99) Abergel, D.; Palmer, A. G. *Concepts Magn. Reson.* **2003**, *19A*, 134.
(100) Trott, O.; Abergel, D.; Palmer, A. G. *Mol. Phys.* **2003**, *101*, 753.
(101) McConnell, H. M. *J. Chem. Phys.* **1958**, *28*, 430.
(102) Rao, B. D. N. *Methods Enzymol.* **1989**, *176*, 279.
(103) Korchuganov, D. S.; Nolde, S. B.; Reibarkh, M. Y.; Orekhov, V. Y.; Schulga, A. A.; Ermolyuk, Y. S.; Kirpichnikov, M. P.; Arseniev, A. S. *J. Am. Chem. Soc.* **2001**, *123*, 2068.
(104) Allerhand, A.; Thiele, E. *J. Chem. Phys.* **1966**, *45*, 902.
(105) Leigh, J. S. *J. Magn. Res.* **1971**, *4*, 308.
(106) Woessner, D. E. *J. Chem. Phys.* **1961**, *35*, 41.
(107) Swift, T. J.; Connick, R. E. *J. Chem. Phys.* **1962**, *37*, 307.
(108) Grey, M. J.; Wang, C.; Palmer, A. G. *J. Am. Chem. Soc.* **2003**, *125*, 14324.
(109) Deverell, C.; Morgan, R. E.; Strange, J. H. *Mol. Phys.* **1970**, *18*, 553.
(110) Trott, O.; Palmer, A. G. *J. Magn. Res.* **2002**, *154*, 157.
(111) Korzhnev, D. M.; Orekhov, V. Y.; Dahlquist, F. W.; Kay, L. E. *J. Biomol. NMR* **2003**, *26*, 39.
(112) Carr, H. Y.; Purcell, E. M. *Phys. Rev.* **1954**, *94*, 630.
(113) Meiboom, S.; Gill, D. *Rev. Sci. Instrum.* **1958**, *29*, 688.
(114) Carver, J. P.; Richards, R. E. *J. Magn. Reson.* **1972**, *6*, 89.
(115) Jen, J. *J. Magn. Reson.* **1978**, *30*, 111.
(116) Rance, M. *J. Am. Chem. Soc.* **1988**, *110*, 1973.
(117) Wang, C.; Palmer, A. G. *J. Biomol. NMR* **2002**, *24*, 263.
(118) Kloiber, K.; Konrat, R. *J. Biomol. NMR* **2000**, *18*, 33.
(119) Dittmer, J.; Bodenhausen, G. *J. Am. Chem. Soc.* **2004**, *126*, 1314.
(120) Orekov, V. Y.; Korzhnev, D. M.; Kay, L. E. *J. Am. Chem. Soc.* **126**, *126*, 1886.
(121) Korzhnev, D. M.; Kloiber, K.; Kanelis, V.; Tugarinov, V.; Kay, L. E. *J. Am. Chem. Soc.* **2004**, *126*, 3964.
(122) Skrynnikov, N. R.; Dahlquist, F. W.; Kay, L. E. *J. Am. Chem. Soc.* **2002**, *124*, 12352.
(123) Eisenmesser, E. Z.; Bosco, D. A.; Akke, M.; Kern, D. *Science* **2002**, *295*, 1520.
(124) Hass, M. A. S.; Thuesen, M. H.; Christensen, H. E. M.; Led, J. J. *J. Am. Chem. Soc.* **2004**, *126*, 753.
(125) Millet, O.; Loria, J. P.; Kroenke, C. D.; Pons, M.; Palmer, A. G. *J. Am. Chem. Soc.* **2000**, *122*, 2867.
(126) Vugmeyster, L.; Kroenke, C. D.; Picart, F.; Palmer, A. G.; Raleigh, D. P. *J. Am. Chem. Soc.* **2000**, *122*, 5387.
(127) Zhang, H.; Neal, S.; Wishart, D. S. *J. Biomol. NMR* **2003**, *25*, 173.
(128) Neal, S.; Nip, A. M.; Zhang, H.; Wishart, D. S. *J. Biomol. NMR* **2003**, *26*, 215.
(129) Dayie, K. T.; Brodsky, A. S.; Williamson, J. R. *J. Mol. Biol.* **2002**, *317*, 263.
(130) Akke, M.; Fiala, R.; Jiang, F.; Patel, D.; Palmer, A. G. *RNA* **1997**, *3*, 702.
(131) Kojima, C.; Ono, A.; Kainosho, M.; James, T. L. *J. Magn. Res.* **1998**, *135*, 310.
(132) Hoogstraten, C. G.; Wank, J. R.; Pardi, A. *Biochemistry* **2000**, *39*, 9951.
(133) Isaacs, R. J.; Rayens, W. S.; Spielmann, H. P. *J. Mol. Biol.* **2002**, *319*, 191.
(134) Dixon, A. M.; Venable, R.; Widmalm, G.; Bull, T. E.; Pastor, R. W. *Biopolymers* **2003**, *69*, 448.
(135) Hoog, C.; Landersjo, C.; Widmalm, G. *Chem.-Eur. J.* **2001**, *7*, 3069.
(136) Almond, A.; Bunkenborg, J.; Franch, T.; Gotfredsen, C. H.; Duus, J. O. *J. Am. Chem. Soc.* **2001**, *123*, 4792.
(137) Martin-Pastor, M.; Bush, C. A. *Biopolymers* **2000**, *54*, 235.
(138) Dangi, B.; Blankman, J. I.; Miller, C. J.; Volkman, B. F.; Guiles, R. D. *J. Phys. Chem. B* **1998**, *102*, 8201.
(139) Bartalesi, I.; Bertini, I.; Rosato, A. *Biochemistry* **2003**, *42*, 739.
(140) Flynn, P. F.; Urbauer, R. J. B.; Zhang, H.; Lee, A. L.; Wand, A. J. *Biochemistry* **2001**, *40*, 6559.
(141) Volkman, B. F.; Lipson, D.; Wemmer, D. E.; Kern, D. *Science* **2001**, *291*, 2429.
(142) Feher, V. A.; Cavanagh, J. *Nature* **1999**, *400*, 289.
(143) Tolkatchev, D.; Xu, P.; Ni, F. *J. Am. Chem. Soc.* **2003**, *125*, 12432.
(144) Mulder, F. A.; Mittermaier, A.; Hon, B.; Dahlquist, F. W.; Kay, L. E. *Nat. Struct. Biol.* **2001**, *8*, 932.
(145) Shapiro, Y. E.; Sinev, M. A.; Sineva, E. V.; Tugarinov, V.; Meirovitch, E. *Biochemistry* **2000**, *39*, 6634.
(146) Shapiro, Y. E.; Kahana, E.; Tugarinov, V.; Liang, Z.; Freed, J. H.; Meirovitch, E. *Biochemistry* **2002**, *41*, 6271.
(147) Tugarinov, V.; Shapiro, Y. E.; Liang, Z.; Freed, J. H.; Meirovitch, E. *J. Mol. Biol.* **2002**, *315*, 155.
(148) Bertini, I.; Carrano, C. J.; Luchinat, C.; Piccioli, M.; Poggi, L. *Biochemistry* **2002**, *41*, 5104.

(149) Mäler, L.; Blankenship, J.; Rance, M.; Chazin, W. J. *Nat. Struct. Biol.* **2000**, *7*, 245.
(150) Inman, K. G.; Baldisseri, D. M.; Miller, K. E.; Weber, D. J. *Biochemistry* **2001**, *40*, 3439.
(151) Spyracopoulos, L.; Gagne, S. M.; Li, M. X.; Sykes, B. D. *Biochemistry* **1998**, *37*, 18032.
(152) Spyracopoulos, L.; Lavigne, P.; Crump, M. P.; Gagne, S. M.; Kay, C. M.; Sykes, B. D. *Biochemistry* **2001**, *40*, 12541.
(153) Gagne, S. M.; Tsuda, S.; Spyracopoulos, L.; Kay, L. E.; Sykes, B. D. *J. Mol. Biol.* **1998**, *278*, 667.
(154) Wang, H.; Hea, Y.; Kroenke, C. D.; Kodukulab, S.; Storch, J.; Palmer, A. G.; Stark, R. E. *Biochemistry* **2001**, *41*, 5453.
(155) Lucke, C.; Fushman, D.; Ludwig, C.; Hamilton, J. A.; Sacchettini, J. C.; Ruterjans, H. *Mol. Cell. Biochem.* **1999**, *192*, 109.
(156) Zhu, L.; Kurian, E.; Prendergast, F. G.; Kemple, M. D. *Biochemistry* **1999**, *38*, 1554.
(157) Constantine, K. L.; Friedrichs, M. S.; Wittekind, M.; Jamil, H.; Chu, C.-H.; Parker, R. A.; Goldfarb, V.; Mueller, L.; Farmer, B. T., II. *Biochemistry* **1998**, *37*, 7965.
(158) Hodsdon, M. E.; Cistola, D. P. *Biochemistry* **1997**, *36*, 2278.
(159) Lu, J.; Cistola, D. P.; Li, E. *J. Mol. Biol.* **2003**, *330*, 799.
(160) Freedberg, D. I.; Wang, Y. X.; Stahl, S. J.; Kaufman, J. D.; Wingfield, P. T.; Kiso, Y.; Torchia, D. A. *J. Am. Chem. Soc.* **1998**, *120*, 7916.
(161) Ishima, R.; Freedberg, D.; Wang, Y.-X.; Louis, J. M.; Torchia, D. A. *Structure* **1999**, *7*, 1047.
(162) Freedberg, D. I.; Ishima, R.; Jacob, J.; Wang, Y.-X.; Kustanovich, I.; Louis, J. M.; Torchia, D. A. *Protein Sci.* **2002**, 221.
(163) Ishima, R.; Louis, J. M.; Torchia, D. A. *J. Mol. Biol.* **2001**, *305*, 515.
(164) Mulder, F. A. A.; Hon, B.; Muhandiram, D. R.; Dahlquist, F. W.; Kay, L. E. *Biochemistry* **2000**, *39*, 12614.
(165) Skrynnikov, N. R.; Mulder, F. A. A.; Hon, B.; Dahlquist, F. W.; Kay, L. E. *J. Am. Chem. Soc.* **2001**, *123*, 4556.
(166) Mulder, F. A. A.; Skrynnikov, N. R.; Hon, B.; Dahlquist, F. W.; Kay, L. E. *J. Am. Chem. Soc.* **2001**, *123*, 967.
(167) Mulder, F. A. A.; Hon, B.; Mittermaier, A.; Dahlquist, F. W.; Kay, L. E. *J. Am. Chem. Soc.* **2002**, *124*, 1443.
(168) Mittag, T.; Schaffhausen, B.; Guenther, U. L. *Biochemistry* **2003**, *42*, 11128.
(169) Finerty, P. J., Jr.; Muhandiram, R.; Forman-Kay, J. D. *J. Mol. Biol.* **2002**, *322*, 605.
(170) Kristensen, S. M.; Siegal, G.; Sankar, A.; Driscoll, P. C. *J. Mol. Biol.* **2000**, *299*, 771.
(171) Kay, L. E.; Muhandiram, D. R.; Wolf, G.; Shoelson, S. E.; Forman-Kay, J. D. *Nat. Struct. Biol.* **1998**, *5*, 156.
(172) Lee, A. L.; Kinnear, S. A.; Wand, A. J. *Nat. Struct. Biol.* **2000**, *7*, 72.
(173) Bracken, C.; Carr, P. A.; Cavanagh, J.; Palmer, A. G. *J. Mol. Biol.* **1999**, *285*, 2133.
(174) Ferreon, J. C.; Hilser, V. J. *Protein Sci.* **2003**, *12*, 982.
(175) Zidek, L.; Novotny, M. V.; Stone, M. J. *Nat. Struct. Biol.* **1999**, *6*, 1118.
(176) Arumugam, S.; Gao, G.; Patton, B. L.; Semenchenko, V.; Brew, K.; Van Doren, S. R. *J. Mol. Biol.* **2003**, *327*, 719.
(177) LeMaster, D. M.; Kushlan, D. M. *J. Am. Chem. Soc.* **1996**, *118*, 9263.
(178) Yang, D. W.; Mittermaier, A.; Mok, Y. K.; Kay, L. E. *J. Mol. Biol.* **1998**, *276*, 939.
(179) Walsh, S. T. R.; Lee, A. L.; DeGrado, W. F.; Wand, A. J. *Biochemistry* **2001**, *40*, 9560.
(180) Evenäs, J.; Malmendal, A.; Akke, M. *Structure* **2001**, *9*, 185.
(181) James, L. C.; Tawfik, D. S. *TIBS* **2003**, *28*, 361.
(182) Osborne, M. J.; Schnell, J.; Benkovic, S. J.; Dyson, H. J.; Wright, P. E. *Biochemistry* **2001**, *40*, 9846.
(183) Schnell, J. R.; Dyson, H. J.; Wright, P. E. *Biochemistry* **2004**, *43*, 374.
(184) Cole, R.; Loria, J. P. *Biochemistry* **2002**, *41*, 6072.
(185) Davis, J. H.; Agard, D. A. *Biochemistry* **1998**, *37*, 7696.
(186) Huang, Y.-T.; Liaw, Y.-C.; Gorbatyuk, V. Y.; Huang, T.-H. *J. Mol. Biol.* **2001**, *307*, 1075.
(187) Martin, J. R.; Mulder, F. A.; Karimi-Nejad, Y.; Van Der Zwan, J.; Mariani, M.; Schipper, D.; Boelens, R. *Structure* **1997**, *5*, 521.
(188) Rozovsky, S.; Jogl, G.; Tong, L.; McDermott, A. E. *J. Mol. Biol.* **2001**, *310*, 271.
(189) Wang, C.; Rance, M.; Palmer, A. G. *J. Am. Chem. Soc.* **2003**, *125*, 8968.
(190) Spector, S.; Raleigh, D. P. *J. Mol. Biol.* **1999**, *293*, 763.
(191) Burton, R. E.; Busby, R. S.; Oas, T. G. *J. Biomol. NMR* **1998**, *11*, 355.
(192) Bracken, C. *J. Mol. Graph. Model.* **2001**, *19*, 3.
(193) Farrow, N.; Zhang, O.; Forman-Kay, J. D.; Kay, L. E. *J. Biomol. NMR* **1994**, *4*, 727.
(194) Tollinger, M.; Skrynnikov, N. R.; Mulder, F. A. A.; Foreman-Kay, J. D.; Kay, L. E. *J. Am. Chem. Soc.* **2001**, *123*, 11341.
(195) Hill, R. B.; Bracken, C.; DeGrado, W. F.; Palmer, A. G. *J. Am. Chem. Soc.* **2000**, *122*, 11610.
(196) Englander, S. W. *Annu. Rev. Biophys. Biomol. Struct.* **2000**, *29*, 213.
(197) Prompers, J. J.; Brüschweiler, R. *J. Am. Chem. Soc.* **2002**, *124*, 4522.
(198) Eliezer, D.; Yao, J.; Dyson, H. J.; Wright, P. E. *Nat. Struct. Biol.* **1998**, *5*, 148.
(199) Eliezer, D.; Chung, J.; Dyson, H. J.; Wright, P. E. *Biochemistry* **2000**, *39*, 2894.
(200) Schwarzinger, S.; Wright, P. E.; Dyson, H. J. *Biochemistry* **2002**, *41*, 12681.
(201) Yao, J.; Chung, J.; Eliezer, D.; Wright, P. E.; Dyson, H. J. *Biochemistry* **2001**, *40*, 3561.
(202) Farrow, N. A.; Zhang, O.; Forman-Kay, J. D.; Kay, L. E. *Biochemistry* **1995**, *34*, 868.
(203) Mok, Y.-K.; Kay, C. M.; Kay, L. E.; Forman-Kay, J. *J. Mol. Biol.* **1999**, *289*, 619.
(204) Yang, D.; Mok, Y.-K.; Muhandiram, D. R.; Forman-Kay, J. D.; Kay, L. E. *J. Am. Chem. Soc.* **1999**, *121*, 3555.
(205) Alexandrescu, A. T.; Jahnke, W.; Wiltscheck, R.; Blommers, M. J. J. *J. Mol. Biol.* **1996**, *260*, 570.
(206) Choy, W.-Y.; Shortle, D.; Kay, L. E. *J. Am. Chem. Soc.* **2003**, *125*, 1748.
(207) Choy, W.-Y.; Kay, L. E. *J. Am. Chem. Soc.* **2003**, *125*, 11988.
(208) Sinclair, J. F.; Shortle, D. *Protein Sci.* **1999**, *8*, 991.
(209) Ackerman, M. S.; Shortle, D. *Biochemistry* **2002**, *41*, 3089.
(210) Stone, M. J.; Gupta, S.; Snyder, N.; Regan, L. *J. Am. Chem. Soc.* **2001**, *123*, 185.
(211) Loria, J. P.; Rance, M.; Palmer, A. G. *J. Biomol. NMR* **1999**, *15*, 151.
(212) Braun, D.; Wider, G.; Wüthrich, K. *J. Am. Chem. Soc.* **1994**, *116*, 8466.

CR030413T